Channeling of Protons in Thin BaTiO₃ Crystals at Temperatures above and below the Ferroelectric Curie Point[*]

D. S. Gemmell and R. C. Mikkelson[†]

Argonne National Laboratory, Argonne, Illinois 60439

(Received 23 February 1972)

The channeling of 3.8-MeV protons in thin (3–20-μ-thick) BaTiO₃ crystals has been studied at 140 °C (i.e., in the cubic paraelectric phase) and at room temperature (i.e., in the tetragonal ferroelectrically polarized phase). The influence of channeling on backscattering yields, on characteristic x-ray production, and on the transmitted protons, has been determined. For the purpose of fitting the data for the cubic phase, the formulas that Barrett found to fit a large range of data on channeling in monatomic crystals were extended to the polyatomic case. The quality of the fit thus obtained is fair, but not as good as those obtained in monatomic lattices. Data are also presented on dechanneling and on the influence of radiation damage on the channeling properties of BaTiO₃. In the polarized tetragonal phase it is found that the channeling properties are strongly affected by the relative orientations of the crystal planes and the polarization of the crystal. The effect of polarization is attributed to the associated high internal electric fields.

I. INTRODUCTION

The theoretical treatment of the channeling of light ions in crystals with fairly simple monatomic lattice structures has now become capable of quantitatively describing channeling effects in yields measured for close-encounter processes. Parameters such as the half-angular widths of the orientation-dependent yields and the fractional yields χ_{min} at the bottoms of these dips can be calculated with precision. For example, these quantities and their dependence on bombarding energy and crystal temperature can be calculated with the expressions given recently by Barrett,[1] and the results generally agree with the experimental values to within 10 or 20%. This level of agreement is obtainable over a wide range of combinations of incident ion, target crystal, temperature, bombarding energy, and crystal orientation.

A more stringent test of channeling theories is to fit data obtained on polyatomic and complex lattice structures. In such structures the atoms present themselves in widely differing combinations and densities in the different crystal directions. Their scattering powers, their charge-screening radii, and their thermal vibration amplitudes are usually different. If a theory is able to achieve a good fit for a large variety of data in these more complicated structures, then it should be relatively easy to fit those special cases in which the atoms are all the same or in which the crystal structure is simple. To date, however, there have been very few detailed studies on channeling in polyatomic or complex structures. Those studies that have been made, including several on backscattering,[2] have employed diatomic crystals.

We have chosen to examine the channeling properties of barium titanate (BaTiO₃) for two main reasons: First, it gives an opportunity to study a triatomic system which, nevertheless, still has a fairly simple lattice structure. Second, the material is a well-known ferroelectric, and it was thought to be of interest to examine the effect of ferroelectricity on channeling.

Above the ferroelectric Curie temperature ($T_C \approx 120$ °C) BaTiO₃ has the cubic perovskite structure shown in Fig. 1. In this cubic (nonpolar) phase, sometimes called the paraelectric phase, the lattice constant is 4.00 Å. Figure 2 shows the atomic arrangements for some of the major (high-symmetry) axial directions in the cubic phase of BaTiO₃. Table I gives the atomic populations and interplanar distances for some of the major planar directions. It is a property

6   1613
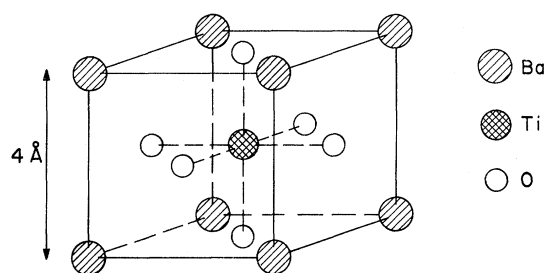
FIG. 1. Unit cell of cubic $BaTiO_3$.

of the perovskite structure that, for any given planar direction (h, k, l) there are always two distinct types of alternating equally spaced atomic planes having different areal densities of the three constituent elements. The crystal atoms always lie on a family of equally spaced planes that are parallel to (h, k, l) and that alternate between the two types. This means that no planar direction has more than one interplanar spacing. Furthermore, it means that the interplanar potential governing planar channeling is always asymmetric. This gives rise to interesting questions as to what the channeling characteristics might be in the various planar directions in $BaTiO_3$. It is of interest to note that when the sum of the Miller indices for a planar direction in a perovskite compound of the type ABO_3 is even, then one of the two alternating types of plane contains only oxygen; when the indices are all odd, one of the types contains only the element B.

Below the ferroelectric Curie point in the temperature range 2–120 °C, $BaTiO_3$ polarizes spon-

TABLE I. Areal densities and interplanar distances D for some major planes in cubic $BaTiO_3$. For any given planar direction, the sheets of atoms always alternate in the pattern $ababab$ ....

Plane	Type	Areal densities (atoms/Å²)			Spacing (Å)
		Barium	Titanium	Oxygen	
(100)	(a)	...	0.062	0.12	2.00
	(b)	0.062	...	0.062	
(110)	(a)	...	...	0.088	1.41
	(b)	0.044	0.044	0.044	
(111)	(a)	...	0.036	...	1.15
	(b)	0.036	...	0.108	
(210)	(a)	...	0.028	0.056	0.89
	(b)	0.028	...	0.028	
(211)	(a)	...	...	0.051	0.82
	(b)	0.025	0.025	0.025	

taneously in a tetragonal phase with lattice constants[3] $a = 3.992$ Å and $c = 4.036$ Å. (The change in lattice constants in going from the cubic to the tetragonal phase has recently been confirmed by proton blocking experiments.[4]) $BaTiO_3$ is considered to be a good example of a displacive ferroelectric, i.e., one in which a substantial fraction of the spontaneous polarization is due to the relative displacements of the ions in the crystal. According to Megaw,[5] one may visualize the structure of tetragonal $BaTiO_3$ as being "derived from the cubic by stretching it slightly parallel to one cube edge and releasing all atoms from their special positions so that they can have small displacements in this direction." The magnitudes of these displacements have been measured by neutron diffraction[6] and have been found to be on the order of 0.1 Å. Figure 3 illustrates the structure of ferroelectrically polarized $BaTiO_3$ in the tetragonal phase. (Below 2 °C, a range of temperatures with which we are not concerned here, there are two other polarized phases with different crystal structures.)

The experiments reported in this paper were performed at two target temperatures. At 140 °C (i.e., in the cubic phase) measurements were made primarily with a view to extending channeling studies to a triatomic system. At room temperature (i.e., in the tetragonal phase) the main aim was to study the interaction between ferroelectricity and channeling. A short preliminary report on some of the data was presented at a recent conference on atomic collision phenomena in solids.[7]

II. EXPERIMENTAL SETUP

The measurements were performed with beams from the 4-MeV Dynamitron accelerator at Argonne National Laboratory. The components of the experimental apparatus (beam line, scattering chamber, detectors, etc.) have been described in
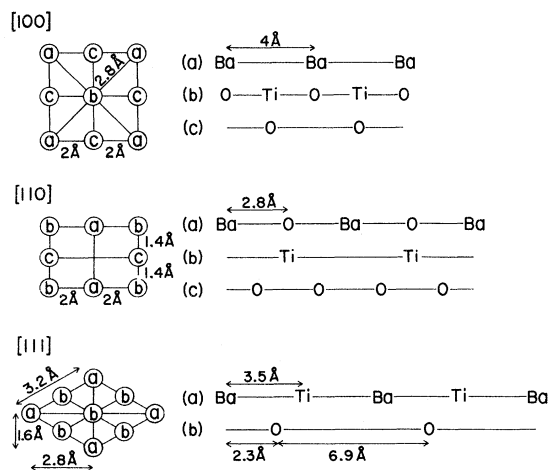

FIG. 2. Atomic arrangements for the [100], [110], and [111] axial directions in $BaTiO_3$. The arrangements shown on the left are end views of the channels, and the letters refer to the individual rows shown on the right.
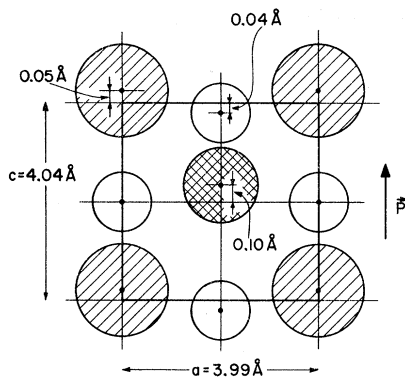
FIG. 3. The atomic displacements (not to scale) of the atoms in the tetragonal phase of $BaTiO_3$. Here the positions are shown projected onto a pseudo-{100} plane which includes the polarization vector $\vec{P}$. For the sake of clarity, two of the four O_{II} atoms in the TiO_6 structure are not shown.

considerable detail in a previous publication.[8] A schematic diagram of the apparatus is reproduced in Fig. 4. The principal features of the system are the good angular resolution available and the high degree of automation and computer control that permit rapid collection and analysis of the data. In the measurements reported here, the divergence of the beam incident on the target crystal was determined by apertures with diameters of 1 mm (first collimator box) and 0.5 mm (second collimator box) spaced 7.54 m apart. Thus the half-angle of the beam divergence was $\sim 0.008°$ and the diameter of the beam spot at the target was ~ 0.5 mm.

Inside the 28-in.-diam scattering chamber, the target crystals were mounted on a goniometer which permitted rotations about three approximately mutually perpendicular axes passing through the target center. These motions were controlled by computer-operated stepping motors which were able to produce rotations in steps as fine as $0.01°$. The entire goniometer could also be translated

over a range sufficient to permit the beam to strike different spots on the target or to miss it altogether if that was required.

A rotating "propeller" which intercepted the beam $\sim 50\%$ of the time was located just inside the entrance to the chamber. Either the beam current falling on this propeller, or the number of particles scattered by it, was monitored for normalization purposes (as explained in Ref. 8). Insertable viewers (e.g., a ZnS screen) for observation of channeling star patterns were located downstream from the chamber.

Particles emerging in the forward direction from the target could be detected over a small angular region by use of a tightly collimated movable detector located inside the XY box shown in Fig. 4. Radiations from the target crystals were measured with three detectors: (i) a silicon surface-barrier detector inserted through a port in the scattering chamber at an angle of $157\frac{1}{2}°$ to the beam direction. Immediately in front of this detector, known as the $P2$ detector, was a collimating aperture of 0.64-cm diameter, and the radially adjustable distance from $P2$ to the target center was normally maintained at 8.3 cm. The $P2$ detector was used in backscattering measurements, and its energy resolution width for 4-MeV protons was about 20 keV. The stopping power of $BaTiO_3$ for 4-MeV protons incident in a random direction is approximately 30 keV/μm. Thus the equivalent target-depth resolution of the $P2$ detector was about 3000 Å. (ii) A lithium-drifted silicon x-ray detector inserted through a port in the scattering chamber at an angle of $135°$ to the beam direction. This Si(Li) detector had an active area of 12 mm² and was located 23.5 cm from the target center. The detector was cooled by liquid nitrogen. The only material between the active portion of the detector and the target was a beryllium foil window 0.001 in. thick. This detector had an energy resolution width of 173 eV (FWHM) for 6.4-keV x rays. (iii) An XY detector. This was also a silicon sur-
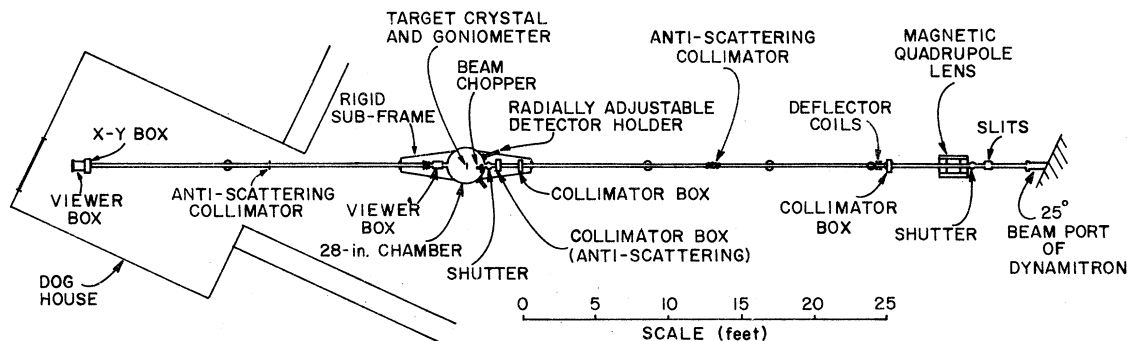

FIG. 4. Schematic diagram showing the beamline, scattering chamber, XY box, etc., at the Argonne 4-MV Dynamitron accelerator.

face-barrier detector with about the same energy resolution as the $P2$ detector. It was located inside the XY box 2.11 m downstream from the target crystal and was collimated by an aperture 0.5 mm square. The XY detector could be moved in steps as small as 25 μm over a plane region normal to the beam direction and about 10 cm square.

When backscattering experiments were performed, the x-ray and backscattered proton spectra were recorded simultaneously in two 4096-channel pulse-height analyzer systems. Selected 512-channel slices of these spectra were stored on magnetic tape. The on-line computer system was programmed to manage the data accumulation and storage (e.g., starting, stopping, and reading the various scalers and pulse-height analyzers; stepping and recording the goniometer positions; providing continuous oscilloscope display of experimental progress). The computer also performed simple analyses of the incoming data, including adding up counts within a selected energy window of pulse-height spectra and making dead-time corrections.

Crystalline samples of $BaTiO_3$ were prepared by a modified version of the technique described by Remeika.[9] A mixture of 27 g of amorphous $BaTiO_3$, 67 g of dry KF, and 0.04 g of Fe_2O_3 in a covered 100-cm^3 platinum crucible was placed inside an oven at 1050 °C. After a "soaking" period of about 6 h, the temperature was reduced to 950 °C over a period of about 3 h, and then the excess molten KF was decanted. After a slow cooling to room temperature, the crucible contained many butterfly twin crystals of $BaTiO_3$. These crystals form as right triangular platelets whose large surfaces are {100} planes. The three edges of the platelets are determined by two {100} planes and one {110} plane. The size, number, and quality of these crystals were found to be critically dependent on such factors as oven temperature, cooling rate, size of the crucible, composition of the initial mixture, etc. After considerable experimentation the procedure outlined above was adopted, and it was found that each run would yield on the order of 20 or 30 usable crystals—typically about 5 mm on a side and about 50 μm thick. These crystals were then washed in water and etched in 170 °C phosphoric acid down to thicknesses in the range 3–20 μm. The resulting target crystals were quite flat over areas large compared to the size of the beam spot and appeared to be fairly free of defects. They gave sharp Laue patterns when examined by x-ray diffraction.

When very thin samples (e.g., < 5 μm thick) were desired, they could also be prepared from thick crystals using an ion-milling process in which the $BaTiO_3$ was removed by sputtering with beams of 6-keV argon ions. Such an argon beam,

with an incident direction 15° from parallel to the crystal surface, produces milling rates of ~ 0.5 μm/h for argon-ion current densities of ~ 70 μA/cm^2. In some cases the crystals were thinned over large areas, while in others they were masked so that only a selected circular area (~ 2 mm^2) was thinned. No evidence of crystal damage or argon-ion implantation was detected for crystals thinned by use of this process.

The crystals were next dc poled by placing them in a high electric field between platinum electrodes in deionized water. In most cases it was possible to pole them into a single ferroelectric domain. To observe the domain boundaries, the crystals were placed between crossed polarizers and looked at microscopically under illumination by approximately monochromatic sodium light.

Each target crystal, cemented in place with conducting silver paste, was mounted on one of the three standard types of target holder shown in Fig. 5. In each case the mount was an aluminum disk (either continuous or split along a diameter) with a resistive electric heater bolted to its back. It was held in place by an insulating boron-nitride ring which fitted into the goniometer. The temperature of the target holder was sensed by a thermocouple which provided the feedback to a stabilizing circuit that controlled the power applied to the heater. The three types of mount were designed for three types of measurements.

The ⟨100⟩ mount, type (a) in Fig. 5, was used for measurements for which the crystal temperature was kept above the Curie temperature T_C and the beam was incident approximately along a ⟨100⟩ direction, i.e., approximately normal to the large surface of the crystal and therefore also to the disk.
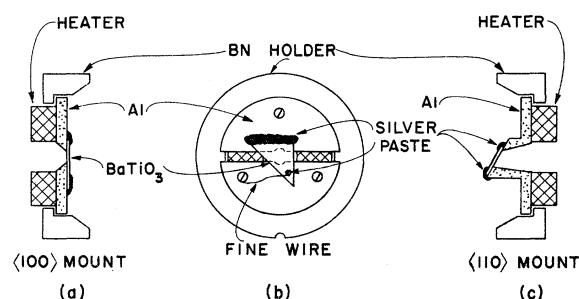
In mounts of type (b), which were designed for

FIG. 5. Target holders used in these experiments. (a) Type used for measurements at temperatures above T_C for beams incident along a ⟨100⟩ direction. (b) Split holder, similar to that shown in (a), which was used for measurements on polarized targets with temperatures above and below T_C. (c) Type used for measurements at temperatures above T_C for beams incident along a ⟨100⟩ direction.

measurements on polarized targets at temperatures both above and below T_C, the aluminum disk was split into two segments by a diametral slot about 1.0 mm wide and each half was bolted to the insulating ring of boron nitride. Most of the area of the crystal lay over this slot. The heating element was also enclosed in an annulus of boron nitride bolted in contact with the two segments, which could thus be heated but were kept electrically insulated from one another. Conducting silver paste cemented one {100} edge of the target crystal to one segment of the mounting disk, and a drop of the paste cemented the opposite tip of the crystal to a fine wire connecting it to the other segment. (The tip of the crystal was not cemented to the disk, since initial attempts to do so were found to crack the crystals on going through the Curie point.) Voltages up to 2 keV could be applied between the two segments of the disk and thus an electric field in a $\langle 100 \rangle$ direction could be applied to the BaTiO₃ crystal.

The $\langle 110 \rangle$ mount [Fig. 5(c)] was similar to type (a) except that the target crystal was mounted at 45° to the plane of the aluminum disk so a $\langle 110 \rangle$ direction in the BaTiO₃ was approximately perpendicular to the plane of the disk.

Close monitoring of the condition of the target was important in these measurements. This included precise temperature measurement and visual observation of the target to check, for example, that it poled into a single domain or, for measurements above the Curie point, that the entire crystal had undergone the transition into the cubic phase. These visual observations were performed by means of the system sketched in Fig. 6. Polarized light from a sodium lamp was directed into the chamber through a window and then (via mirror No. 1) through the target crystal. Then mirror No. 2 (with a small hole in it to permit passage of the ion beam) reflected the transmitted light through another window and a crossed polarizer and finally into a microscope giving an image of the target magnified 30 times. Mirror No. 1 could be withdrawn for measurements on ions transmitted in the forward direction. The crosshairs of the microscope were aligned on the beamspot at the target by including a slight smear of activated ZnS powder on a nonvital section of the target assembly and then translating the goniometer so that the ion beam struck this fluorescent material. The microscope and mirror No. 2 could then be precisely adjusted to focus on the now-visible beamspot. The goniometer was then translated back so that the beam passed through the center of the BaTiO₃ crystal. In this way exactly the crystal area being irradiated could be visually monitored with high precision. At temperatures below the Curie point, the domain struc-
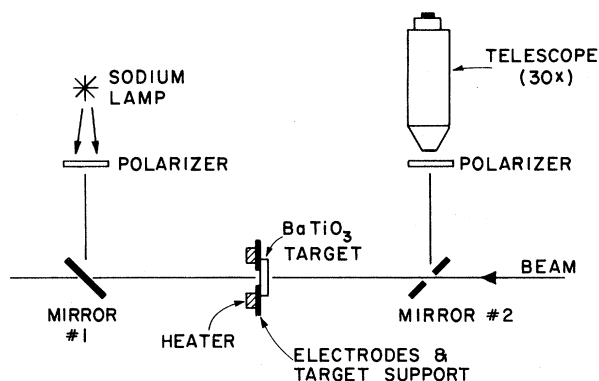

FIG. 6. Schematic diagram showing the arrangement for observing domain structure in ferroelectric BaTiO₃ by use of monochromatic polarized sodium light.

ture of the target could be directly observed.

III. RESULTS AND DISCUSSION

A. Cubic Phase $(T > T_C)$

Measurements on channeling in the cubic phase of BaTiO₃ were performed with target temperatures maintained at 140 °C. Figure 7 shows energy spectra measured by the $P2$ detector and the x-ray detector for 3.8-MeV protons incident in a random direction upon a 4-μm-thick BaTiO₃ crystal. For target thicknesses less than about 8 μm, the $P2$ detector was able to completely separate the spectral peak due to backscattering from oxygen. For thicknesses greater than 8 μm, a background-subtraction technique was used to extract the oxygen yield. We were unable to produce satisfactory targets thin enough (~1.5 μm) to permit separation of the peak due to Ti. Attempts to separate the Ti data by background subtraction were unsuccessful because of the poor statistics. It was found that the BaTiO₃ crystals were very susceptible to radiation damage, and this imposed a limitation on the statistical accuracy obtainable in the backscattering data.

Figures 8 and 9 show data obtained on axial channeling along the [100] and [110] directions in BaTiO₃. Each of these figures shows five sets of data. In order from bottom to top, these are as follows: (i) the number of counts obtained in a window set on the high-energy edge of the peak in the $P2$ spectrum. These counts (which correspond to backscattering from barium) are plotted against the angular position of the goniometer as it is scanned linearly in angle through a range within which a major crystal direction is brought into coincidence with the incident beam direction. The window setting for each of these two diagrams is fairly narrow and reflects the channeling properties within about the first micron of crystal penetration. (ii) Data obtained in a similar fashion
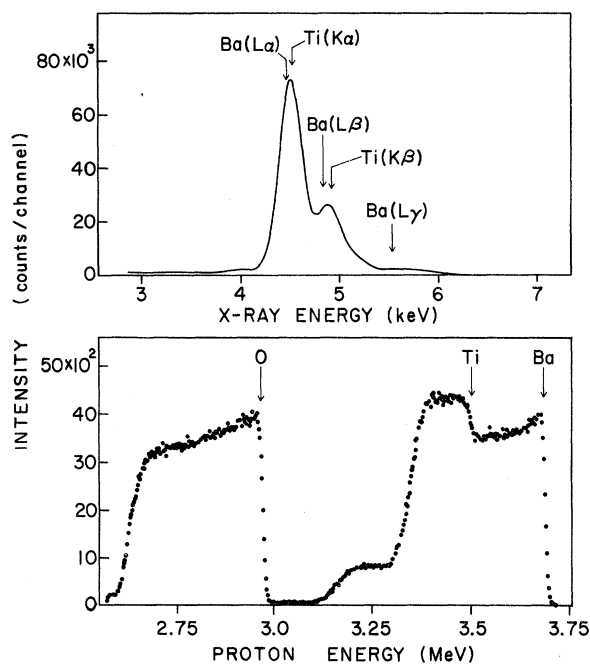
FIG. 7. Energy spectra recorded by the Si (Li) detector (top) and $P2$ (silicon surface-barrier) detector (bottom) for characteristic x rays and backscattered ($157\frac{1}{2}$°) protons when a 4-μm-thick $BaTiO_3$ crystal was bombarded with 3.8-MeV protons.

for backscattering ($P2$ detector) from oxygen atoms in the target. (iii) A similar goniometer scan, except that the counts now are the total number of low-energy ($\sim$4–6-keV) x rays measured by the Si(Li) detector. (iv) A goniometer scan in which the counts are those in a window set on the high-energy portion of the spectrum in the XY detector. The detector was kept fixed on the beam axis for these measurements. Thus the data in the figures represent the channeled (low-energy-loss) portion of the transmitted beam. It was found that the shapes and angular widths of the curves thus obtained were somewhat dependent on the width of the window set on the spectrum and on the target thickness. (v) Data obtained much as in (iv) except that now the target crystal was held fixed in such an orientation that the beam entered along a major crystal direction, and the XY detector was moved in a linear scan over a range that included this direction.

1. Values of $\psi_{1/2}$ and χ_{min} for Axes

The measured values for χ_{min} (the ratio of the minimum yield to the random yield) and $\psi_{1/2}$ (the half-angular width at half-minimum or at half-maximum) are summarized in Table II. The values given for the backscattering data are those found by extrapolation to zero target thickness

(i. e., the windows in the $P2$ spectra were moved to successively higher energies and the values of χ_{min} and $\psi_{1/2}$ corresponding to zero energy loss were determined). In this way the depth dependence of these quantities (mostly a consequence of dechanneling processes) was eliminated. This explains why some of the $\psi_{1/2}$ values given in Table II are slightly higher than those shown in the figures.

The calculated values for $\psi_{1/2}$ given in Table II for the backscattering cases were determined by taking the empirical formula that Barrett[1] found to fit his Monte Carlo calculations for protons in a tungsten crystal and then generalizing it to the case of a polyatomic crystal. For axial channeling, Barrett found that a very good fit both to the temperature-dependent results of his calculations and to an impressively large set of experimental data involving a wide range of (monatomic) target
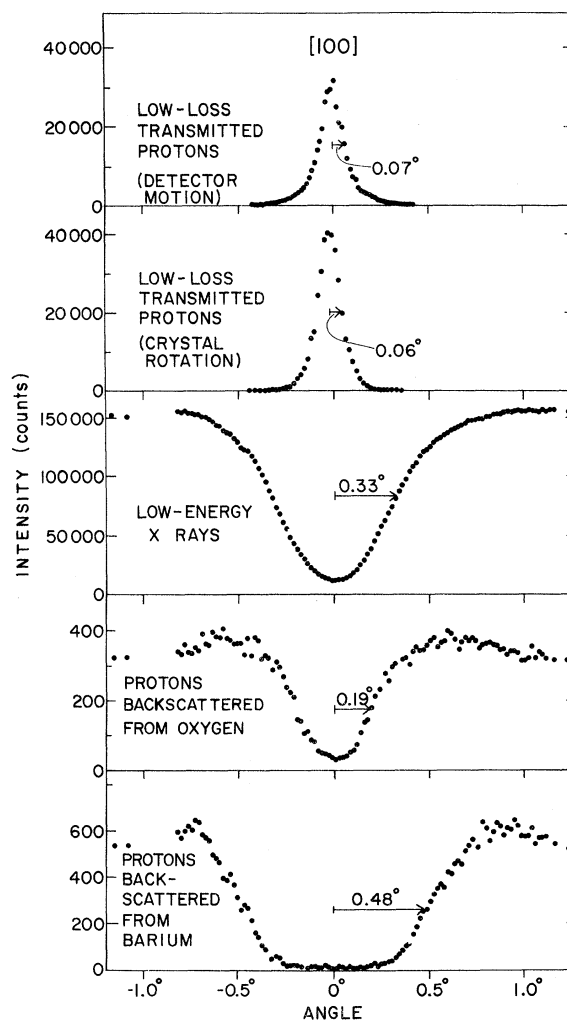

FIG. 8. Angular dependence for channeling along the [100] axis in a cubic $BaTiO_3$ crystal of 4-μm thickness.
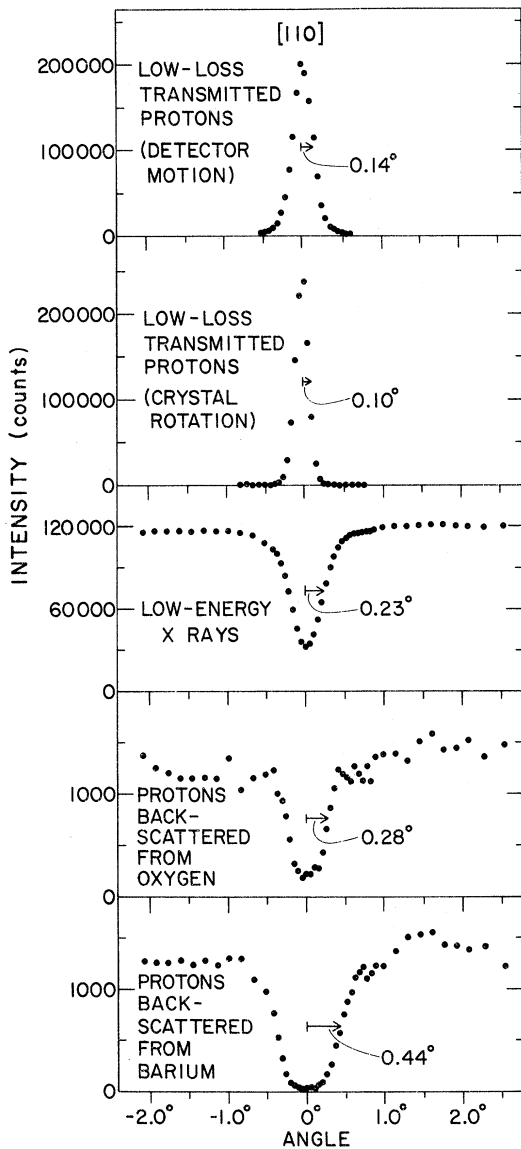
FIG. 9. Angular dependence for channeling along the [110] axis in a cubic BaTiO₃ crystal of thickness 16 μm along the incident beam direction.

crystals and incident ions could be obtained with an expression that may be written

$$\psi_{1/2} = 0.80 \left[V_{rs}(1.2u_1)/E \right]^{1/2} , \qquad (1)$$

where u_1 is the rms value of one spatial component of the thermal vibration amplitude, E is the energy of the incident ion beam, and $V_{rs}(r)$ is the continuum potential energy computed at a distance r from a static atomic row when one employs Molière's approximation to the Thomas-Fermi potential for the ion-atom interaction. [10]

The formalism to describe channeling in polyatomic crystals was developed by generalizing Eq. (1). In doing this, we have arbitrarily chosen

to interpret the $1.2u_1$ as the minimum distance of closest approach to an atomic row for the trajectories of channeled particles. The factor 0.80 is interpreted as the ratio of the half-angle $\psi_{1/2}$ to the critical angle ψ_c. A polyatomic crystal may have several types of row in any particular axial direction, and the linear density of each atomic species varies from one type of row to another. We further assume that a single critical angle exists for each type of row and that the critical angle for any particular row j is determined by the distance of closest approach to this row. This distance is $1.2u_{1\,max}^{j}$, where $u_{1\,max}^{j}$ is the largest of the u_1 values for atomic species in that row.

With these assumptions and in analogy with Eq. (1), the expression for the half-angle $\psi_{1/2}^{j}$ for the jth type of row in a given axial direction is found to be

$$\psi_{1/2}^{j} = 0.80 \{ [\textstyle\sum_i V_{rs}^{ij}(1.2u_{1\,max}^{j}) - V_0]/E \}^{1/2} , \qquad (2)$$

where $V_{rs}^{ij}(r)$ is the continuum potential energy due to the ith atomic species in the jth type of row. Again we use Molière potentials evaluated for static rows. The sum over i in Eq. (2) extends over all atomic species in the crystal. The term V_0 represents the minimum potential in the open channels between rows. The V_0 term affects the calculated half-angles very little for heavy elements and for monatomic lattices; it is not introduced by Barrett. [1] It can have a pronounced effect in polyatomic lattices, however, especially for rows containing light elements when other rows contain heavy elements.

The calculated values of $\psi_{1/2}$ given in Table II were derived from Eq. (2) using the amplitudes for the thermal vibrations of BaTiO₃ at 140 °C. These were taken from the work of Pedersen, [11] who found $u_1(Ba) = u_1(O) = 0.074$ Å; $u_1(Ti) = 0.101$ Å. The agreement between calculated and measured values of $\psi_{1/2}$ for axial backscattering is good, although the calculated values tend to be a little lower than the measured ones. For oxygen the agreement is best for those cases in which $\psi_{1/2}$ is calculated for monatomic rows (i.e., for row c as shown in Fig. 2 for the [100] and [110] axes). These monatomic rows of oxygen contain twice as many oxygen atoms as do the polyatomic rows. If one simply adds up the weighted values of the calculated half-angles for oxygen, one obtains 0.23° and 0.29° for the [100] and [110] axial directions, respectively. This near-perfect agreement with the measured values is probably fortuitous in view of the poorer agreement found in the case of barium.

As a consequence of the assumption that each type of row has its own characteristic critical angle, particles traversing a polyatomic crystal can have transverse energies lying in a range such that the particles are channeled with respect to

TABLE II. Measured and calculated parameters for axial channeling in cubic $BaTiO_3$. The experimental measurements were made with a target temperature of 140 °C and 3.8-MeV protons. The calculated values (enclosed in parentheses) were obtained from Eq. (2) for $\psi_{1/2}$ and from Eq. (4) for χ_{min}.

	Crystal rotated by goniometer							Scan by moving XY detector	Stopping power
	Backscattered protons				Characteristic x rays		Fixed XY detector		$\dfrac{(dE/dx)_{ch}}{(dE/dx)_{rand}}$
	Barium		Oxygen						
Axis	$\psi_{1/2}$	χ_{min}	$\psi_{1/2}$	χ_{min}	$\psi_{1/2}$	χ_{min}	$\psi_{1/2}$	$\psi_{1/2}$	
[100]	0.51°	0.010	0.23°	0.12	0.32°	0.14	0.06°	0.07°	0.53
	(0.43°)	(0.011)	$\frac{2}{3}$a: (0.19°)	(0.08)	Ba: (0.43°)	(0.01)	Weakest[b]: (0.19°)		
			$\frac{1}{3}$a: (0.32°)		Ti: (0.32°)	(0.03)	Hyper[b]: (0.05°)		
[110]	0.44°	0.015	0.28°	0.14	0.22°	0.24	0.10°	0.14°	0.52
	(0.40°)	(0.011)	$\frac{2}{3}$a: (0.23°)	(0.05)	Ba: (0.40°)	(0.01)	Weakest[b]: (0.23°)		
			$\frac{1}{3}$a: (0.40°)		Ti: (0.22°)	(0.09)	Hyper[b]: (0.09°)		

[a]The notations $\frac{2}{3}$ and $\frac{1}{3}$ denote the atomic sheets that, respectively, contain $\frac{2}{3}$ and $\frac{1}{3}$ of the oxygen atoms. These values are discussed in Sec. III A 2.

[b]"Weakest" and "hyper" refer to the values calculated for the cases of the weakest rows in the axial directions and for hyperchanneled protons, respectively.

some rows but travel randomly with respect to others. This aspect of channeling in polyatomic or complex lattice structures is one that has important implications. For example, the minimum yields χ_{min} observed in backscattering are strongly affected. Reference to the potential contours plotted in Fig. 10 illustrates this point.

Let us consider the minimum yield for backscattering from oxygen and suppose the beam is incident parallel to the [100] axial direction. In the [100] direction, oxygen atoms occur in two types of rows (rows b and c in Fig. 2). Row b consists of alternating titanium and oxygen atoms; row c contains only oxygen. For the minimum

yield for backscattering from oxygen, for example, the contribution to χ_{min} from rows of type c will consist of two parts. The first is a contribution from beam ions that are incident on c rows with impact parameters less than some value r_{min}. Let $V^c_{rs}(r_{min})$ denote the static continuum potential at this distance. The second contribution is from beam ions that are incident on a- and b- type rows with impact parameters less than the distances r_a and r_b at which the continuum potential is equal to $V^c_{rs}(r_{min})$. These portions of the beam will have sufficiently high transverse energies to be traveling randomly with respect to the "weak" rows of type c, even though they may possibly be
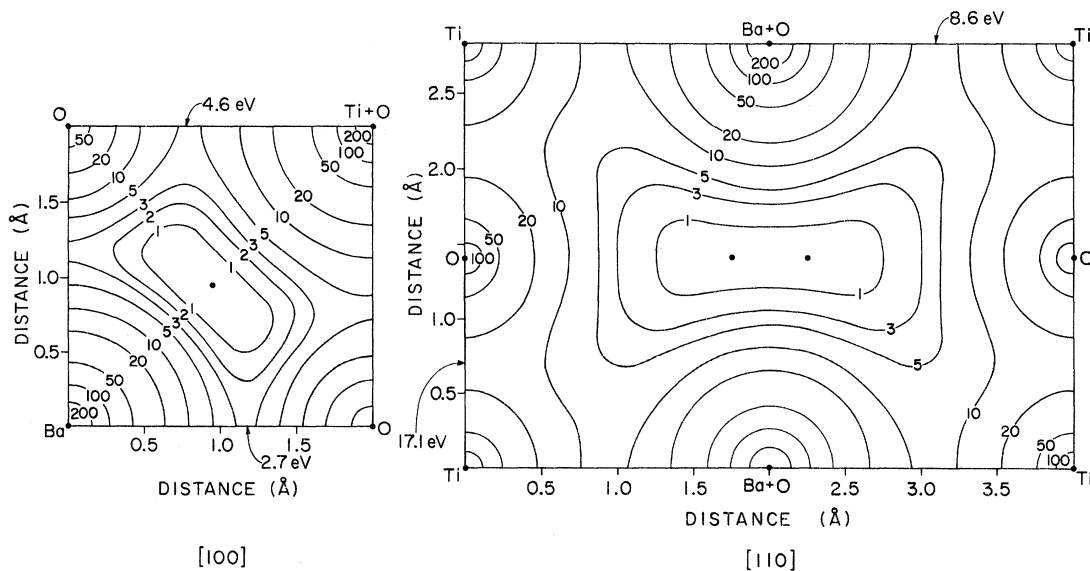

[100] [110]

FIG. 10. Potential-energy contour diagrams for [100] and [110] directions in cubic $BaTiO_3$, as calculated by use of the static continuum form of the Molière potential function (Ref. 10). Only one-quarter of the cross-sectional area of the unit cell is presented for the [100] direction.

channeled with respect to the "strong" rows a and b.

Contributions to χ_{min} from oxygen atoms in type-b rows will similarly come in part from b rows and in part from the other two types of rows.

In choosing a value for r_{min}, we have again used Barrett's results[1] as a guide. For the incident proton energy (3.8 MeV) in the present experiments, the expression Barrett found to fit his Monte Carlo calculations for monatomic lattices can be written to a good approximation as

$$\chi_{min} = 3n\pi u_2^2 , \qquad (3)$$

where n is the areal density of the rows being presented to the incident beam and $u_2 = \sqrt{2}u_1$ is the rms displacement of the atoms due to thermal vibrations in the plane normal to the axis. In extending Eq. (3) to the polyatomic case, we have chosen to interpret it as meaning that the beam ions that are incident parallel to the row and that have impact parameters less than $\sqrt{3}u_2$ with respect to the row will not be channeled but will travel randomly with respect to such rows and thereby will contribute to the minimum yield. Formally, the axial minimum yield in backscattering from the ith atomic species in the crystal is given by

$$\chi_{min}^i = \sum_j \chi_{min}^{ij} = \sum_j \left(f_{ij} \sum_k n_k \pi r_{jk}^2 \right) , \qquad (4)$$

where χ_{min}^{ij} is the contribution to χ_{min}^i from rows of type j, the fraction f_{ij} of the ith atomic species occurs in rows of type j so $\sum_j f_{ij} = 1$, the summations over both k and j in Eq. (4) are over the different types of row, n_k is the areal density of the type-k rows in a plane normal to the beam direction, and the radii r_{jk} are defined by

$$\sum_i V_{rs}^{ik}(r_{jk}) = \sum_i V_{rs}^{ij}(\sqrt{3} u_{2\,max}^j) , \qquad (5)$$

where $u_{2\,max}^j$ is the largest of the values of u_2 for elements occurring in the jth row.

Thus, in our example of the [100] minimum yield of protons backscattered from oxygen in BaTiO₃, we set r_{min} equal to $\sqrt{3}u_2^o$, where u_2^o is the value of u_2 for oxygen (the only atomic species occurring in rows of type c). The potential $[V_{rs}^c(r_{min}) - V_0]$ is then found to be 33 eV. The radii r_a and r_b corresponding to this potential are both about 0.48 Å, a value almost twice as large as $r_{min} = 0.18$ Å. This example serves to illustrate the strong effects that one row can have on another. Rows of type a do not contain any oxygen, but they cause a larger contribution to the χ_{min} value for oxygen than do rows of type c, which contain only oxygen. This type of reasoning is supported by the experimental observation that the minimum yields for atoms occurring in "weak" rows are higher than those for atoms in "strong" rows.

The level of agreement between measured and

calculated values of χ_{min} given in Table II is of the same order as that obtained by Barrett[1] in comparing his results with experiment. The agreement is best for barium in the [100] direction and gets poorer for oxygen and for the [110] direction.

2. Values of $\psi_{1/2}$ and χ_{min} for Planes

Figures 11 and 12 show some results for measurements on channeling in the (100) and (110) planes of BaTiO₃. The data are arranged in the same format as that used for Figs. 8 and 9. A striking feature noticeable in comparing Figs. 11 and 12 is the similarity of the dips observed for barium but the great difference for the oxygen
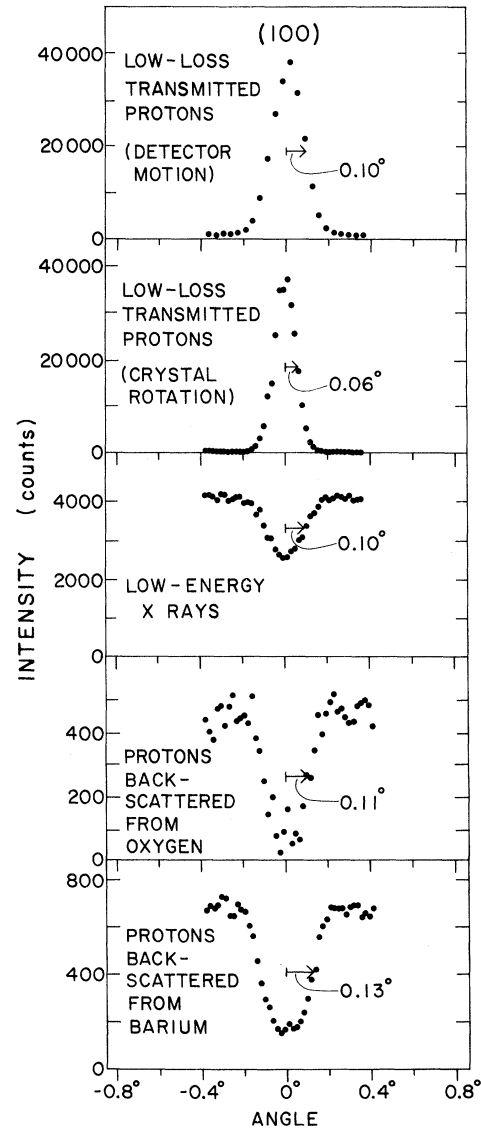

FIG. 11. Angular dependence for channeling along the (100) planes in a cubic BaTiO₃ crystal of 13-μm thickness.
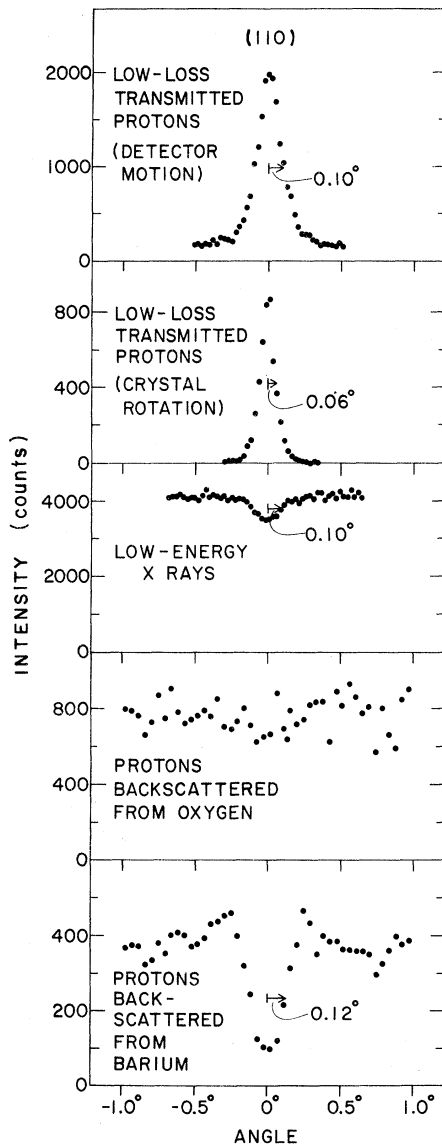
FIG. 12. Angular dependence for channeling along the (110) planes in cubic $BaTiO_3$. Backscattering data in the lowest two panels were obtained from a 50-μm-thick crystal. Data in the upper three panels were obtained from a 12-μm-thick crystal.

data. In Table III the results of measurements (again extrapolated to zero target thickness) and calculations for planar channeling in cubic $BaTiO_3$ are summarized. The calculated values of $\psi_{1/2}$ are again obtained from a formula deduced by generalizing Barrett's expression[1] to polyatomic crystals. Barrett found that his planar Monte Carlo calculations and also a wide variety of experimental data on monatomic crystals could be fitted with the expression

$$\psi_{1/2} = 0.72 \, [V_{ps}(1.6 u_1)/E]^{1/2} , \qquad (6)$$

where $V_{ps}(r)$ is the summed static continuum planar potential (Molière approximation) adjusted to be zero at the midpoint between planes and evaluated at a distance r from a plane. In extending Eq. (6) to the polyatomic case, we have chosen to interpret it to mean that the minimum distance of closest approach (measured from channeled trajectories to a plane) is $1.6 u_1$. We interpret the factor 0.72 to be the ratio of the half-angle $\psi_{1/2}$ to the critical angle ψ_c.

In a polyatomic crystal a given planar direction may have several types of sheets of atoms in which the constituent elements combine in differing areal densities. We make the assumption that each of these types of sheets has its own characteristic critical angle for channeling. We further assume that for a sheet of a given type j, the minimum distance of closest approach for channeling is equal to $1.6 u_{1\,max}^j$, where $u_{1\,max}^j$ is the largest of the values of u_1 for those elements occurring in that type of sheet of atoms.

With these assumptions and in analogy with Eq. (6), the half-angle $\psi_{1/2}^j$ for a type-j atomic sheet in a given planar direction is found to be

$$\psi_{1/2}^j = 0.72 \{ [\textstyle\sum_i V_{ps}^{ij}(1.6 u_{1\,max}^j) - V_0]/E \}^{1/2} , \qquad (7)$$

where $V_{ps}^{ij}(r)$ is the static continuum potential energy (Molière approximation) due to the ith atomic species in the jth type of atomic sheet. The term V_0 is introduced in order to make the minimum potential at some point (not necessarily the midpoint) between adjacent planes equal to zero. (For cases more complex than $BaTiO_3$, it may be necessary to introduce this term in a more general fashion in order to describe more complicated modes of planar channeling—e. g., when the minimum potentials in adjacent planar channels are not equal.)

For the calculated values given in Table III, the potentials $V_{ps}^{ij}(r)$ were determined by adding the contributions from the five nearest-neighbor planes on each side of the region for which the potential was being calculated. A constant potential was then subtracted to make the potentials at the minima equal to zero. The potentials thus determined for the (100), (110), and (111) planes of $BaTiO_3$ are shown in Fig. 13. It is apparent that, while the interplanar potentials in the (100) channels are almost symmetric, in the cases of the (110) and (111) channels they are strongly asymmetric. This indicates the possibility that two types of channeling may occur in the (110) and (111) planar directions. First, channeling can occur solely between neighboring planes—this mode should have a small critical angle because of the shallowness of the associated potential well. Second, channeling may take place between neighboring "strong" planes— i. e., between the sheets of Ba+ Ti+ O atoms in the case of the (110) and between the sheets of Ba

TABLE III. Measured and calculated parameters for planar channeling in cubic $BaTiO_3$. The experimental measurements were made with a target temperature of 140 °C and 3.8-MeV protons. The calculated values (enclosed in parentheses) were obtained from Eq. (7) for $\psi_{1/2}$ and from Eq. (9) for χ_{min}.

	Crystal rotated by goniometer							Scan by moving XY detector	Stopping power
	Backscattered protons				Characteristic x rays		Fixed XY detector		$\dfrac{(dE/dx)_{ch}}{(dE/dx)_{rand}}$
Plane	Barium		Oxygen						
	$\psi_{1/2}$	χ_{min}	$\psi_{1/2}$	χ_{min}	$\psi_{1/2}$	χ_{min}	$\psi_{1/2}$	$\psi_{1/2}$	
(100)	0.14°	0.17	0.11°	0.20	0.09°	0.63	0.07°	0.09°	0.54
	(0.13°)	(0.23)	$\frac{2a}{3}$: (0.11°)	(0.24)	Ba: (0.13°)	(0.23)	(0.11°)		
			$\frac{1a}{3}$: (0.13°)		Ti : (0.11°)	(0.24)			
(110)	0.12°	0.26	~ 0.06°	~ 0.8	0.12°	0.72	0.06°	0.10°	0.68
	(0.12°)	(0.17)	$\frac{2a}{3}$: (0.05°)	(0.49)	Ba: (0.12°)	(0.17)	(0.05°)		
			$\frac{1a}{3}$: (0.12°)		Ti: (0.12°)	(0.17)			
(111)	0.11°	0.34	0.10°	0.35	0.09°	~ 0.9	0.07°	0.10°	0.91
	(0.11°)	(0.20)	(0.11°)	(0.20)	Ba: (0.11°)	(0.20)	(0.03°)		
					Ti: (0.03°)	(0.64)			

[a]The notations $\frac{2}{3}$ and $\frac{1}{3}$ denote the atomic sheets that, respectively, contain $\frac{2}{3}$ and $\frac{1}{3}$ of the oxygen atoms. These values are discussed in Sec. III A 2.

+ 3O atoms in the case of the (111). Such a mode should have a relatively large critical angle, but would be expected to decay rapidly with penetration depth into the crystal since these channeled trajectories would have a high probability of encounter with the atoms contained in the intervening "weak" planes.

The planar half-angles calculated for backscattering according to the expression in Eq. (7) are in excellent agreement with the measured values (as seen in Table III). For the (100) and (110) orientations of the planes, the oxygen atoms occur in both types of planar sheet and therefore, for these cases, two calculated values of $\psi_{1/2}$ are given in Table III. In each instance the best agreement with the experimentally determined values is obtained for the sheets containing $\frac{2}{3}$ of the oxygen atoms. For the (110) orientation of the planes, one might expect to be able to observe two critical

angles in the case of backscattering from oxygen. There is some suggestion of this in the data, but the statistical accuracy (limited by radiation damage in the target) is too poor to allow any definite conclusions.

No theoretical expression in the literature can accurately predict minimum yields for planar channeling in monatomic crystals. Most calculated values (e. g., those in Refs. 1 and 12–14) are about half as large as the experimentally determined ones. Therefore, Table III lists only the values of χ_{min} determined from a generalization of the rough estimate given by Lindhard, [12] who suggested that the values for monatomic crystals could be approximated by

$$\chi_{min} = 2a/d_p , \qquad (8)$$

where a is the Thomas-Fermi screening radius, d_p is the interplanar distance, and the planes are
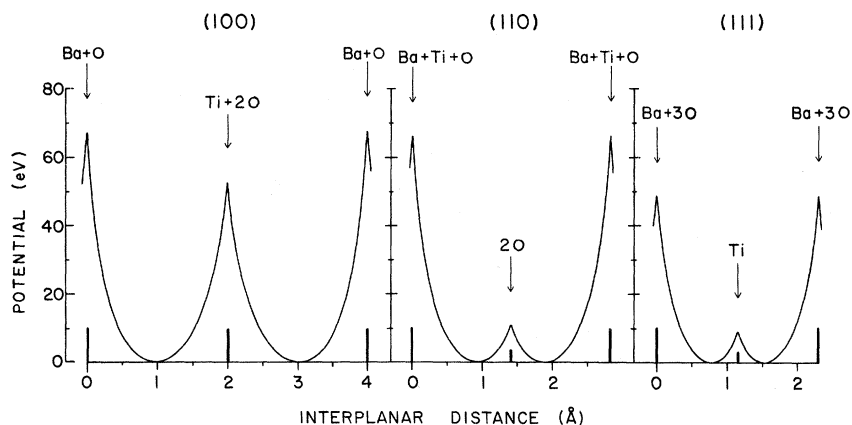

FIG. 13. Continuum-approximation potentials calculated for the (100), (110), and (111) planes in $BaTiO_3$. A static lattice is assumed and the ion-atom potential used is the Molière approximation to the Thomas-Fermi potential.

assumed to be equally spaced. Then reasoning of the type used to generalize from Eq. (3) to Eqs. (4) and (5) in the case of axial channeling can be applied to generalize Eq. (8) to the case of polyatomic planar channeling. The resulting expression for the minimum yield for backscattering from the ith atomic species in the crystal is

$$\chi^i_{min} = \sum_j \chi^{ij}_{min} = \sum_j \left(g_{ij} \sum_k 2m_k t_{jk}\right) , \qquad (9)$$

where χ^{ij}_{min} is now the contribution to the planar minimum yield from the jth type of atomic sheet in the given planar direction and g_{ij} is that fraction of the ith atomic species occuring in sheets of type j ($\sum_j g_{ij} = 1$). The summations over j and k in Eq. (9) are both summations over the different types of atomic sheet, m_k is the linear density of sheets of the type k in a plane normal to the beam, and the distances t_{jk} are defined by

$$\sum_l V^{ik}_{ps}(t_{jk}) = \sum_l V^{ij}_{ps}(a^j_{max}) , \qquad (10)$$

where a^j_{max} is the largest of the values of a for those elements occurring in the jth atomic sheet.

As expected, the measured and calculated values of planar χ_{min} do not agree especially well. From Table III one sees that in some instances the calculated values are too high and in others too low. One encouraging point is that the calculated value (0.5) for backscattering from oxygen in the (110) direction is significantly higher than the values for the other directions—in harmony with the experimental observation that the (110) value (~0.8) is much higher than the other measured χ_{min} values given in Table III.

It is interesting to note that in the (111) planar orientation the measured values of $\psi_{1/2}$ and χ_{min} for barium and oxygen backscattering are identical within the associated errors. In the (111) direction all of the oxygen atoms occur in the same atomic sheets as the barium atoms. Thus the experimental result supports the idea that the incident particles may be regarded as either channeled or not channeled with respect to a given type of atomic sheet and that each type of sheet has a single value of the critical angle associated with it.

3. Values of $\psi_{1/2}$ and χ_{min} for X Rays

The L x rays from barium and the K x rays from titanium lie close enough in energy, and their energy spectra are complex enough (as seen in Fig. 7), that it was not possible in these experiments to separate the x-ray yields from the two elements. (The cross sections for the production of titanium K x rays and barium L x rays are approximately equal for 3.8-MeV protons.) Thus the x-ray data shown in Figs. 8, 9, 11, and 12 and in Tables II and III are those obtained for the sum of all x rays detected in the energy range 4–6 keV. Unlike the backscattering data, the x-ray data do not carry de-

tailed depth information. That is, by simply detecting an x ray of a certain energy, one gains very little information about how deep below the crystal surface the x ray was generated. One knows that as the energy of the incident ions is degraded during passage through the crystal, the cross section for production of characteristic x rays decreases.[15] The efficiency for detection of x rays also falls off (approximately exponentially) with depth in the crystal as a consequence of absorption in the crystal. On the other hand, the dechanneling of the incident beam makes an increasing number of particles available for x-ray-producing collisions as the beam penetrates deeper into the crystal. Thus the values of $\psi_{1/2}$ and χ_{min} given in Tables II and III for x rays do not pertain only to the surface layers of the crystal, but are modified by the considerations outlined above.

For the x-ray spectrum shown in Fig. 7, the average value of the mean free path for absorption in BaTiO$_3$ is about 7.5 μm. Thus the probability for detecting x rays from depths greater than 10 or 20 μm becomes very small. In traversing distances of this magnitude, the incident beam (3.8-MeV protons) suffers an energy loss of roughly 500 keV. The results of Bissinger $et\ al.$[15] show that the cross section for production of K x rays from titanium falls only by about 11% when the bombarding proton energy is reduced from 3.8 to 3.3 MeV. Thus the main factors influencing the depths from which x rays are detected are the absorption in the crystal (mean free path about 7.5 μm) and dechanneling. (The mean free paths for channeling of 3.8-MeV protons in BaTiO$_3$ range from about 10 μm downwards, depending on the particular crystal orientation being considered, as will be discussed further in Sec. III A 5.)

The calculated values of $\psi_{1/2}$ and χ_{min} given in Tables II and III for x rays are calculated from Eqs. (2), (4), (7), and (9). That is, they are "surface" values which do not take account of depth effects such as have just been described. Since the experimental values represent the summed titanium K and barium L x rays and since the production cross sections for the x rays from the Ti and Ba are roughly equal, it may not be unreasonable to compare the measured values with the calculated values averaged for the two elements. (This procedure would be expected to be most valid when the values of $\psi_{1/2}$ and χ_{min} for the Ti and Ba are not very different.) For axial channeling (Table II) one finds that, unlike the results obtained for backscattering, the measured values of $\psi_{1/2}$ for x rays are lower than the calculated ones. This is understandable in terms of dechanneling. Those particles initially channeled on entering the crystal but having large transverse energies are the ones that are expected to dechannel most rapidly. These

particles, then, have the best chance of producing x rays in the first few microns below the crystal surface (where the corresponding detection efficiency is high). From these considerations one can readily see that as the average transverse energy of the channeled beam is raised by increasing the angle ψ between crystal axis and beam direction, the yield of x rays detected will rise more rapidly than will the yield of backscattered particles detected from the surface region. For the planar case a similar effect exists (Table III). These depth-dependent effects also account for the large values of χ_{min} for x rays. It is interesting to note the abnormally high value (~ 0.9) for the (111) planar orientation. This is most likely due to the effect of the "weak" planes containing only titanium (the planes corresponding to the small interplanar peak in Fig. 13).

Roth et al.[16] have studied how the x-ray yields observed in proton bombardment of NaCl crystals are affected by dechanneling. Dechanneling is discussed further in Sec. III A 5.

4. Measurements on Transmitted Protons

It has long been established that the stopping power for channeled ions is lower than that for randomly traveling ions.[17] Tables II and III give the ratios of channeled stopping power to random stopping power for protons incident parallel to various axes and planes in BaTiO₃. These ratios are very closely the same for the [100] and [110] axial directions (Table II) and also equal to the value in the (100) planar direction (Table III). These observations are in keeping with the notion[18] that the stopping power for axially channeled ions is equal to the stopping power for ions channeled in the most open plane (i. e., in the planar channel with the lowest stopping power) intersecting in the axis in question.

Although the energy spectrum for transmitted protons is fairly simple when the detector (the XY detector in our case) lies on the beam axis and when the beam is incident either parallel to a channel or at some large angle to it (random incidence), the situation is far from simple when the detector lies off the beam direction or when the beam is incident at some small nonzero angle relative to the channeling direction. This is illustrated in Figs. 14–17, which may be regarded as showing a series of "slices" through a three-dimensional space in which the number of transmitted protons striking the XY detector is plotted as a function of two parameters: "angle" and detected energy. In Figs. 14 and 16, the "angle" is the angle between the incident beam direction and an axial channel direction (the [100] in Fig. 14 and the [110] in Fig. 16) and in Figs. 15 and 17 it is the angle between the XY detector and the beam direction, the beam being incident parallel to an axial channel (the [100] in Fig. 15 and the [110] in Fig. 17).

It is apparent that the widths and shapes of the curves in Figs. 14–17 vary in a complex fashion with energy and angle. For example, in Fig. 14 the angular widths seem to get larger for higher detected energies, whereas in Fig. 16 the trend is in the opposite direction. However, such simple observations about the data are not very meaningful since the results are strongly dependent on the thickness of the target crystal. Thus the data given in Table II for the XY detector were recorded for crystal thicknesses of 4 μm (for the [100] axis) and 12 μm (for the [110] axis) and with energy windows set on the upper edge of the channeled peak. The data shown in Figs. 14–17 were recorded with crystal thicknesses of 11 μm (for the [100] axis) and 16 μm (for the [110] axis).

The channeled-particle trajectories themselves are probably far from simple. Reference to Fig. 10 would suggest that for different ranges of the initial transverse energy the trajectories could follow widely differing paths through the crystal. Since the experimental angular resolution is small compared to the critical angles involved, these differences may result in the complex behavior observed. One can imagine, for example, that for a beam incident parallel to the [110] axial direction, a large fraction of the beam would have initial transverse energy less than ~ 9 eV. This fraction would initially be "proper" channeled[12] or hyperchanneled[19]; i. e., it would be confined to a single open channel of the type illustrated in Fig. 10. This component has an abnormally low rate of energy loss and is rather fragile[19]; i. e., it is easily bumped into a normal channeling mode. In addition there is a range of transverse energies from approximately 9 to 17 eV in which particle trajectories would be free to migrate around the "strong" rows of barium-plus-oxygen (quasihyperchanneling?). The portion of the channeled beam with transverse energies above about 17 eV would be able to overcome all potential barriers between adjacent rows and would correspond to the normal channeled component. Even this "normal" component can be subdivided according to whether the transverse energy is in one of three ranges corresponding to the requirements for channeling with respect to the three types of rows. Similar considerations apply to the [100] direction.

Each of these subcomponents of the channeled beam would have its own characteristic rate of energy loss and its own dechanneling rate (or rate of transferring into other subcomponents). The initial population of these subcomponents is strongly dependent on the initial beam direction, which determines the initial distribution in transverse energy. From the energies and distances involved,
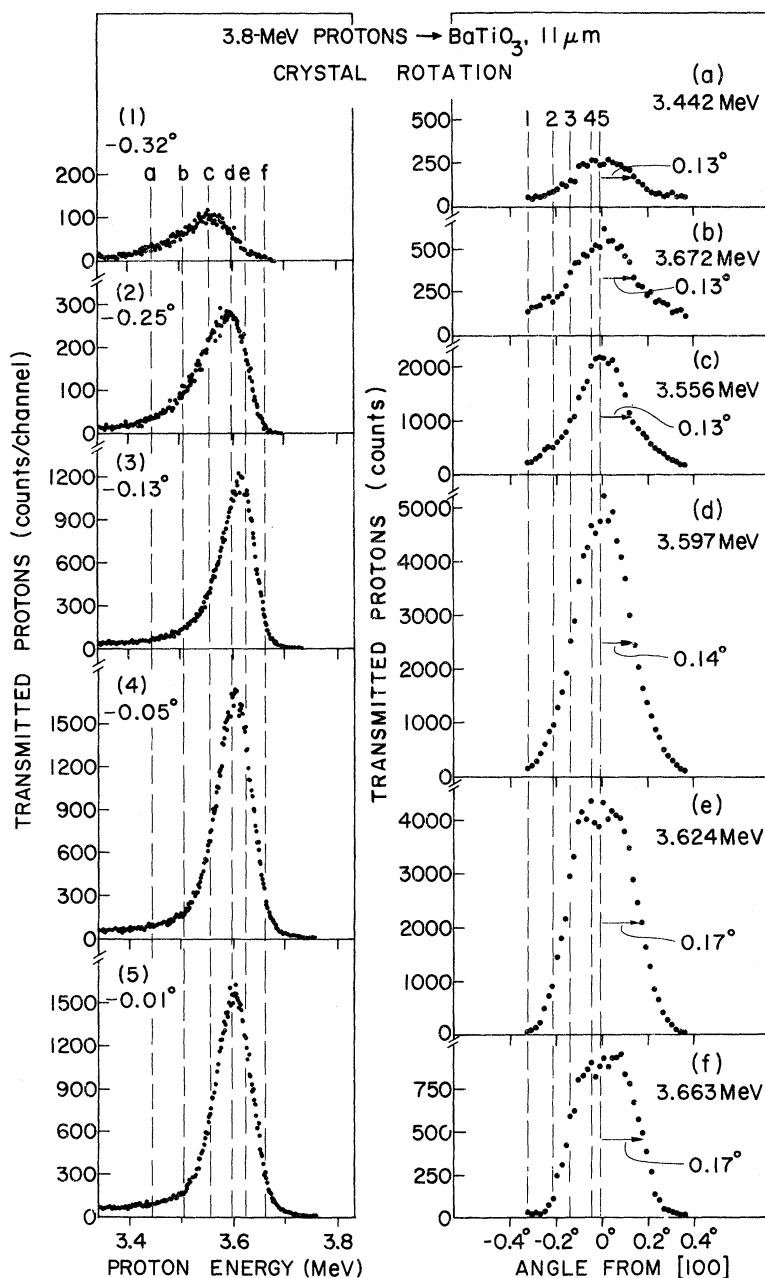
FIG. 14. Energy and angle dependence of transmitted protons when 3.8-MeV protons are incident approximately parallel to the [100] direction in an 11-μm-thick BaTiO₃ crystal. The number of incident protons was the same for each crystal orientation. The letters on the vertical lines in the curves at the left designate the transmitted proton energies at which the angular scans with the same letters were taken; the numbers on the vertical lines in the angular scans at the right correspond similarly to the numbers of the energy spectra at the left. These energy spectra were obtained with the XY detector held collinear with the beam direction while the goniometer swept the [100] axis of the crystal through the beam direction. The angular distributions at the right result from setting a window ($\Delta E = 3.3$ keV) on the energy spectra of the transmitted protons and thus represent protons that have suffered selected energy losses during their passage through the crystal. The energy loss of the 3.442-MeV emergent protons [curve (a)] is the same as for protons that penetrate the crystal in a random direction. The half-widths at half-maximum are indicated on the angular scans.

one can estimate that the particle trajectories "oscillate" in the longitudinal direction with "wavelengths" on the order of a few hundred to a few

thousand angstroms. Thus in traversing a crystal ~ 10 μm thick, axially channeled particles may make a few tens to a few hundreds of collisions

with rows. This is scarcely a sufficiently large number to achieve statistical equilibrium in the population of the subcomponents corresponding to the various ranges of transverse energy. This would account for the strong depth dependence of the observed distributions. One might expect that the depth dependence would be more marked for thinner crystals and less so for thicker ones.

Data obtained with the *XY* detector were recorded for axial channeling in BaTiO$_3$ crystals with thicknesses of 4, 9, 11, 12, and 16 μm. No

definite trend with thickness could be determined for curves of the type shown in Figs. 14–17. In all cases, the measured angular widths were smaller than the smallest angular widths measured in backscattering. This seems to be good evidence that the beam ions that are initially channeled only with respect to strong rows are rapidly dechanneled by the "random" collisions with weak rows. Of the portion initially channeled with respect to the weak rows, those particles with largest transverse energies will be the first to dechannel.
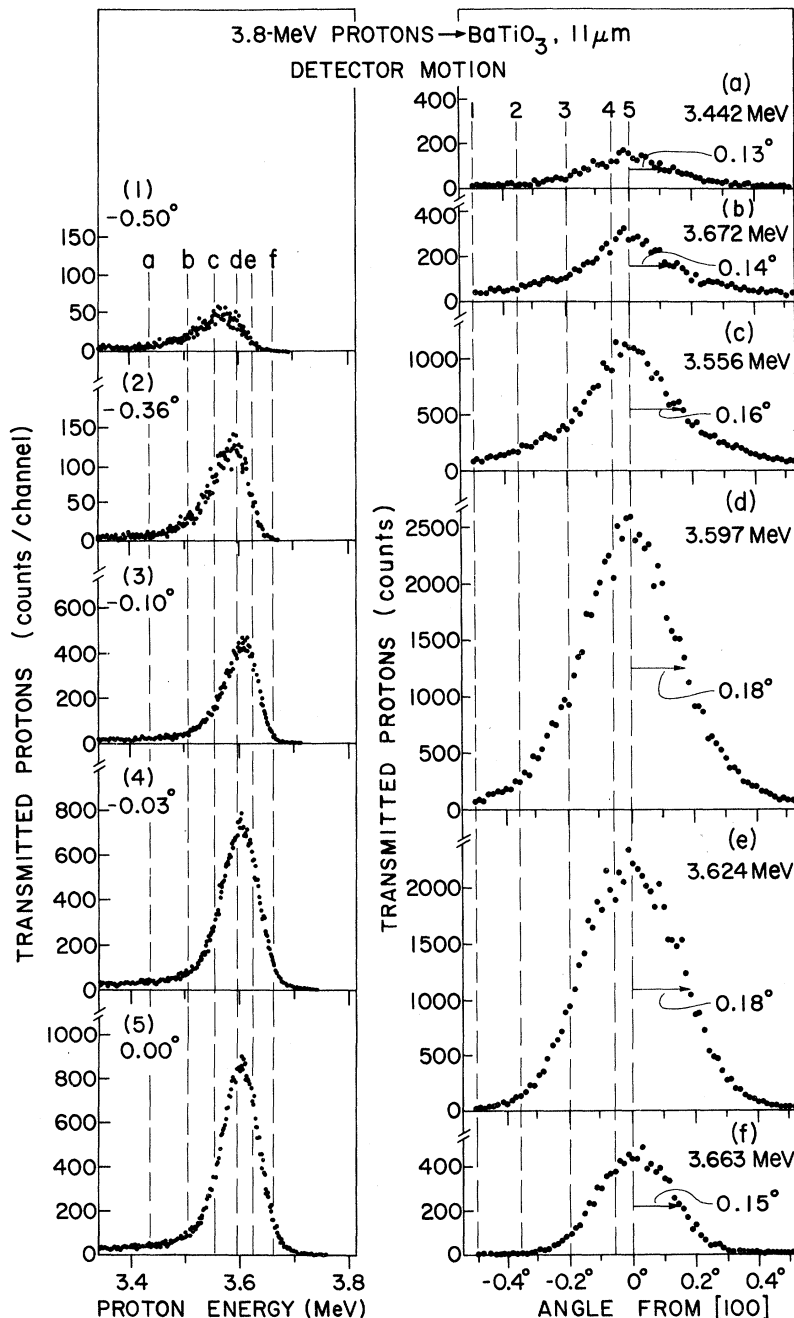

FIG. 15. Energy and angular dependence of transmitted protons when 3.8-MeV protons are incident exactly along the [100] direction in an 11-μm-thick BaTiO$_3$ crystal. The angular dependence results from scanning the *XY* detector along a straight line that intersects the direction of the aligned beam and crystal axis. All other details are as described for Fig. 14.
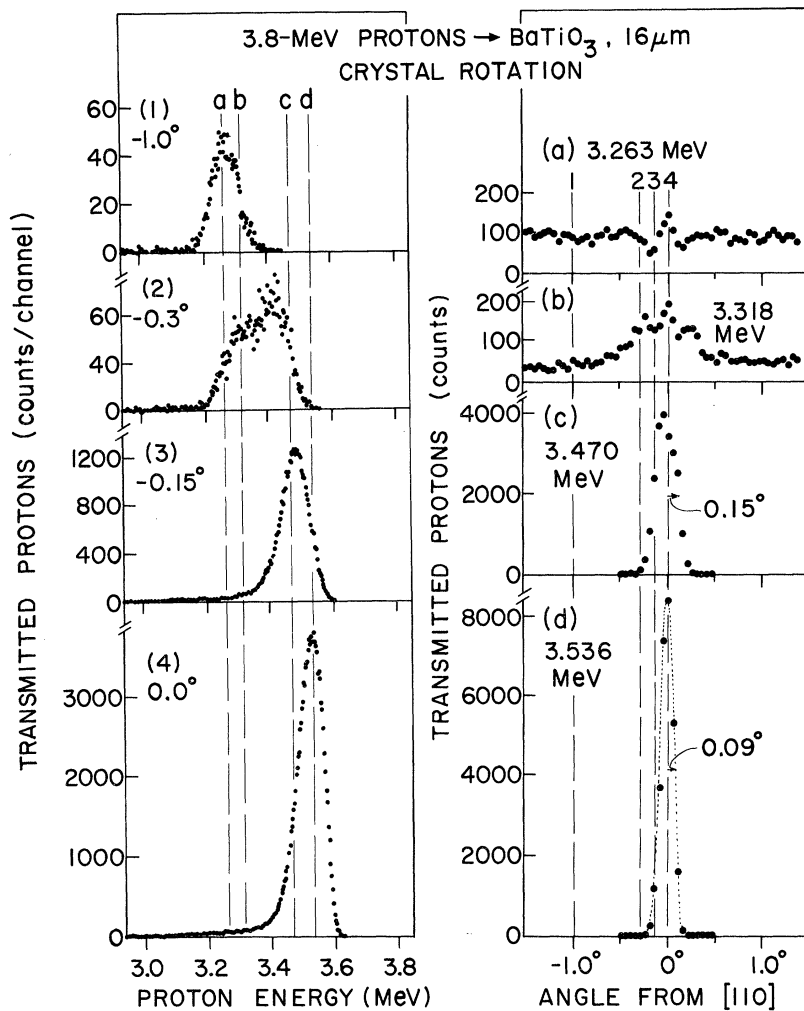
FIG. 16. Energy and angle dependences similar to those in Fig. 14 except that the channeling is along the [110] axis, the crystal thickness measured in the direction of the beam is now 16 μm, and the width of the energy window for the angular scans is 6.1 keV. The energy lost by protons emerging from the crystal with an energy of 3.263 MeV is the same as for protons that penetrate this crystal in a random direction.

The channeled component persisting through the crystal to depths of several microns will then tend to have transverse energies less than the maximum allowable for channeling with respect to weak rows. (Table II lists calculated values for the weakest rows and also, for comparison, the values for the hyperchanneled components of the beam.)

Similar results were obtained for the planar case. Here the depth dependence was not quite as pronounced as for axial channeling—probably as a result of the faster dechanneling rates leading more rapidly to statistical equilibrium of the channeled beam. The calculated values in Table III are those for the "weak" planes; one might expect the channeling between "strong" planes to die out much more rapidly with depth into the crystal.

In all cases the angular widths measured with detector motion (e. g., Figs. 15 and 17) were larger than the corresponding ones measured for rotation of the target crystal (e. g., Figs. 14 and 16). This can be understood in the following terms. For protons incident parallel to an axis,

the initial distribution in transverse energy is optimum for maximum penetration of the beam into the crystal. As the beam passes through the crystal, this distribution spreads towards higher transverse energies as a result of multiple scattering. At the exit from the crystal, this spread translates itself into a spread in the emergence angles seen by the XY detector (detector motion). For the case of crystal rotation while the detector is kept fixed in the beam direction, several factors tend to reduce the angular width observed. The initial channeled fraction decreases with incidence angle and a similar factor again reduces the fraction of the beam leaving the crystal in the direction of the detector. Also, the dechanneling rate increases with incidence angle and thus further reduces the transmission of channeled particles through the crystal.

5. Dechanneling

As an initially channeled beam travels through a crystal, the channeled fraction decreases steadily with depth. This dechanneling effect is thought to

be caused by electronic and nuclear multiple scattering, which gradually shift the initial distribution of transverse energies toward higher values. When the transverse energy of a particle in the beam exceeds some critical value, it is considered to be dechanneled. This effect has been the subject of much recent investigation, [20-23] predominantly for simple monatomic target crystals. For further details see, for example, Refs. 7, 12, 20-23, and references cited therein.

The strong influence of dechanneling upon the quantities given in Tables II and III has already been discussed in Secs. IIIA1-4. Further information on dechanneling can be obtained from plots of the backscattering minimum yields χ_{min} as functions of the penetration depth x. Figure 18 is such a plot for backscattering from barium and oxygen for channeling along the [100] and [110] axial directions in BaTiO₃. The depth scale was calculated on the assumption that the values of dE/dx for the incoming and for the backscattered particles are equal to the random values (obtained from the tabulation of Williamson *et al.*[24]). That is, the value of χ_{min} is obtained by taking the ratio of intensities of channeled and nonchanneled backscattered particles having the same detected energies. This approach is commonly used in extracting dechanneling data from backscattering measurements. It is, however, open to question and will be discussed further below. As Fig. 18 shows, the dechanneling rate is slightly higher for the [110] direction than for the [100] direction. In Fig. 19 the quantity $1 - \chi_{min}$, which may be interpreted as the channeled fraction, is plotted on a logarithmic scale as a function of depth.

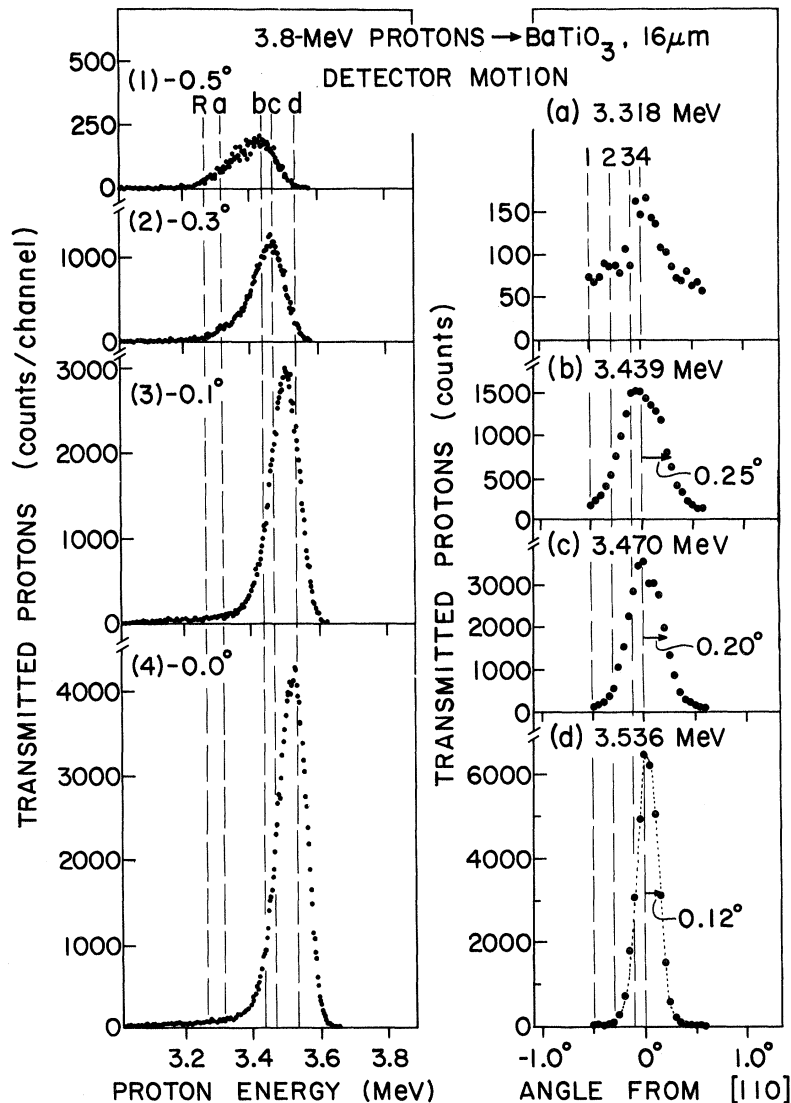Figure 20 shows a similar plot of data for planar

FIG. 17. Energy and angle dependences similar to those in Fig. 15 except that the crystal is now fixed with the [110] axis parallel to the incident beam, the crystal thickness in the beam direction is 16 μm, and the energy window is 6.1 keV wide. The vertical line marked R in the energy spectra indicates the energy E = 3.263 MeV at which protons emerge after traversing the crystal in a random direction. No angular scan is presented for that energy.
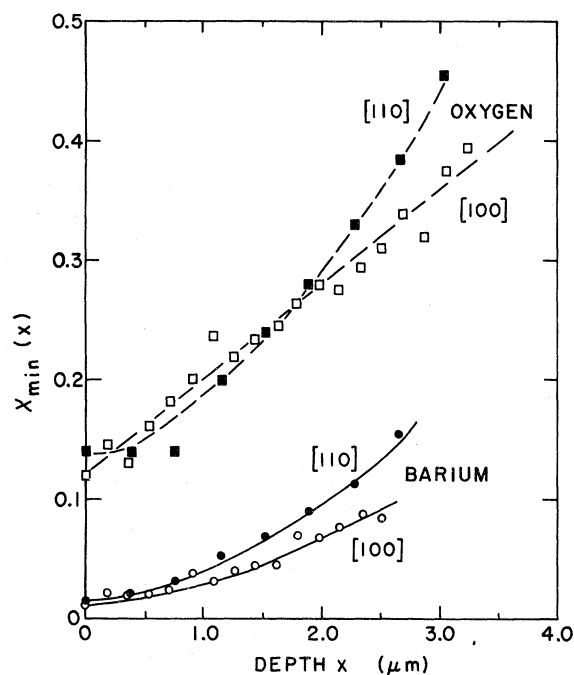
FIG. 18. Backscattering yields from barium and oxygen for 3.8-MeV protons incident along [100] and [110] axes in $BaTiO_3$. The depth scale presented here assumes identical stopping powers for channeled and random particles.

channeling. Here one sees that for depths greater than about 1 μm the channeled fraction appears to decrease in an approximately exponential fashion. Also shown in Fig. 20 are fits to the data by use of the diffusion formalism of Feldman et al.[25] For four of the six sets of data in Fig. 20, the fitted curves were obtained by taking the measured sur-
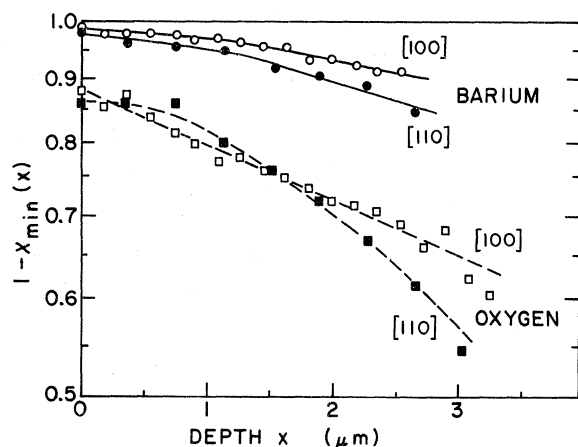

FIG. 19. Depth dependence of the channeled fractions $1 - \chi_{min}$ for axial channeling. The depth scale was determined on the assumption of identical stopping powers for channeled and random protons.
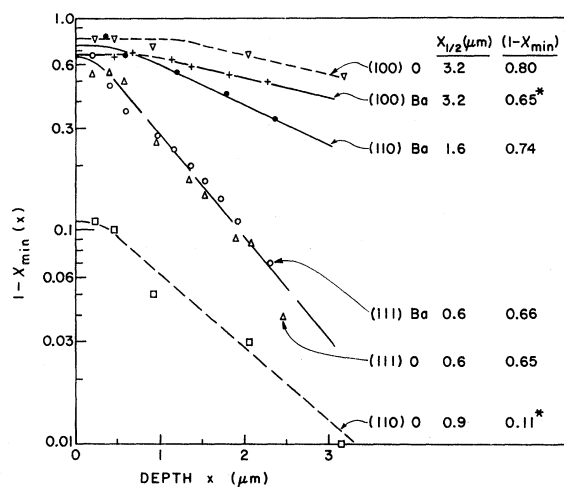

FIG. 20. Depth dependence of the channeled fractions $1 - \chi_{min}$ for planar channeling. The curves through the data points were obtained by substituting the indicated values of $x_{1/2}$ and $1 - \chi_{min}$ (the channeled fraction at the crystal surface) into the diffusion formalism of Feldman et al. The starred values of $1 - \chi_{min}$ disagree with the χ_{min} values given in Table III but are required to give good fits to the experimental data. The depth scale was determined on the assumption of identical stopping powers for channeled and random protons.

face values of χ_{min} as given in Table III and adjusting the dechanneling rates to give the best fits to the data. For the other two cases [barium in the (100) and oxygen in the (110) direction] the value of χ_{min} had to be adjusted in order to fit the data. Figure 20 also lists the fitted values of $x_{1/2}$, the half-thickness for dechanneling. The dechanneling rates measured for barium and oxygen in the (111) planar direction are the same within the experimental accuracy.

Unlike the situation for monatomic crystals, in polyatomic structures one can measure dechanneling rates for the different atomic species in the target. Following the reasoning of Secs. III A 1 and III A 2, one may speak of the dechanneling properties of the various types of rows or atomic sheets in a given crystal direction. The dechanneling rate measured for a particular atomic species would then be determined by considering the various types of row or sheet in which that species occurs. As the mean transverse energy of a proton increases as it traverses the crystal, the critical values for the weakest rows or sheets would be exceeded first. One might therefore expect that the weakest rows and sheets would have the fastest dechanneling rates. Thus, in the case of oxygen in the [100] and [110] axial channels (Fig. 18), for example, one might anticipate that the value of χ_{min} as a function of depth would rise rapidly for small depths (as a consequence of the dechanneling

with respect to the weak rows containing only oxygen) and then more slowly at greater depths (because the dechanneling rate is smaller for the strong rows also containing oxygen). That the data do not show such a trend indicates that this is too simple a picture of the process. A more complete description would have to include the interactions between different types of row or sheet and also include the effect of rechanneling (which is expected to be significant when χ_{min} is large[23]).

It should be pointed out that the depth scales given in Figs. 18–20 are somewhat uncertain. They were obtained by what may be termed the "usual" method; i.e., the rate of energy loss for the incident beam was taken to be equal to the random rate (as was done, for example, in Refs. 20–23). However, the incident particles are channeled for some undetermined fraction of the depth traversed before backscattering. The rate of energy loss in the channeled part of the trajectory is also not determined. If the particles are well channeled, the rate of energy loss may perhaps be as low as 0.3 of the random value. However, such particles would have a low probability for dechanneling. For dechanneling particles the channeled stopping powers may come close to or even exceed the random value.[26]

A further problem frequently encountered in extracting dechanneling rates from data on backscattering from light atoms such as oxygen is that the backscattering-yield curves often exhibit pronounced nuclear resonance effects. The bombarding proton energy of 3.8 MeV in the present work was in large part chosen because the differential cross section for the $^{16}O(p, p)\,^{16}O$ reaction at backward angles is a fairly flat function of bombarding energy in this region.[27]

6. Radiation Damage

The BaTiO₃ crystals proved to be extremely sensitive to damage induced by the incident proton beam. These damage effects limited the statistical accuracy obtainable in backscattering measurements on the cubic phase. (Even higher damage rates altogether precluded such measurements on the tetragonal phase.) The symptoms of the damage were a degradation and eventual disappearance of the "star patterns" of the transmitted beam observed on a ZnS screen and the gradual disappearance of the backscattering minima. This latter effect is illustrated in Figs. 21 and 22.

Figure 21 shows backscattering spectra (same number of incident protons for each spectrum) obtained for a BaTiO₃ crystal at three different stages of irradiation. The crystal, which was thin enough (1.7 μm) for the complete separation of the three elements in backscattering, was oriented so that the incident beam was parallel to the [100] axial di-
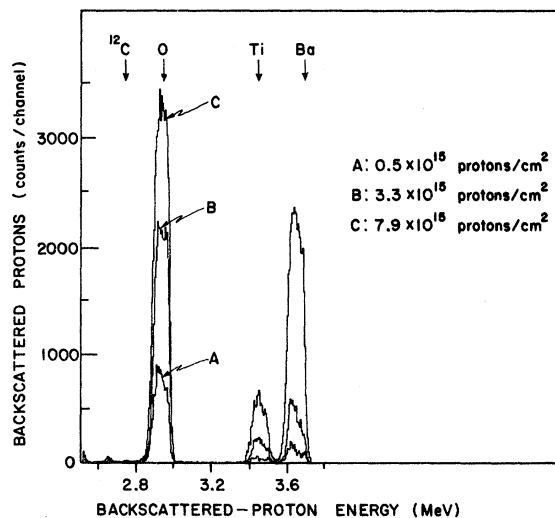

FIG. 21. Pulse-height spectra showing the increase in backscattering as channeling in the [100] direction is progressively destroyed by radiation damage. The three spectra, each produced by the same number of incident protons, were recorded after the crystal (thickness 1.7 μm) has received the three indicated beam doses.

rection. The target temperature was 140 °C.

Spectra similar to those of Fig. 21 were recorded as the target was progressively irradiated. Figure 22 shows the total number of counts under the peak due to scattering by each of the three elements, plotted as a function of the proton dose. After the remarkably small dose of about 6×10^{15} protons/cm² (roughly equivalent to one proton per channel in the [100] direction), no sign of channeling could be observed in either backscattering or transmission. (It is of interest to note that similar doses have been found to destroy channeling in crystals of alkali halides.[16,28])

While studies of electron, neutron, and γ irradiation of BaTiO₃ have been reported,[29–33] there appears to be no conclusive evidence one may use to identify the defect mechanisms responsible for the various electrical and mechanical changes observed. Most of these studies have been carried out on ferroelectric crystals at temperatures below 100 °C, where it is found that a fast neutron flux nvt $\approx 10^{19}$ cm⁻² will produce a phase transition from tetragonal to cubic structure.[32,33] Tentative explanations of hysteresis-loop measurements, which reveal a decrease in saturation polarization P_s with increasing electron or γ doses, involve displacements of oxygen atoms.[29,30,33]

Crystal defects induced by proton irradiation would be expected to cause dechanneling. The data of Fig. 18 show that the dechanneling rates measured for barium and for oxygen are not very different in the [100] direction. Therefore, the fact
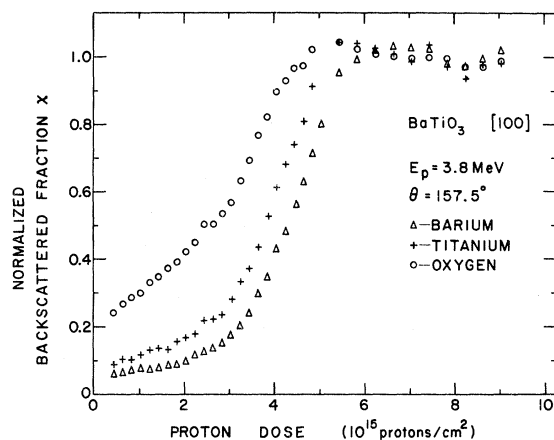
FIG. 22. Dose dependence for the backscattering of protons incident along the [100] crystal axis. The curve for backscattering from any given element was obtained by placing an energy window over the appropriate portion of the pulse-height spectra shown in Fig. 21. The resulting yields are normalized to the saturation values that result for large doses.

that the backscattering yield for oxygen climbs much more rapidly with dose than does that for barium (Fig. 22) indicates the possibility that the predominant effect of the irradiation is the production of interstitial oxygen atoms. Flux-peaking effects[34] could then account for the high backscattering yields.

Two other experiments were performed to see if surface effects were causing the channeling properties to disappear as the dose increased. First, a crystal was irradiated in the beam until it showed no channeling. Then it was removed from the scattering chamber and about 2 μm was removed from each side of the crystal by ion milling. (It was found that the irradiated section of the crystal milled at a much higher rate than the unirradiated section.) The crystal was then reinserted and it was immediately found still not to have any channeling properties. Second, a back-reflection Laue x-ray picture was taken of an unirradiated crystal. It gave sharp spots indicating a fairly perfect crystal. The crystal was then irradiated in the proton beam until it showed no channeling properties whatsoever. A further Laue picture was taken (the x-ray beam had a diameter of 0.010 in. and was carefully located on the center of the 0.020-in.-diam spot of proton irradiation). The second Laue picture showed a slight broadening of the spots but nevertheless indicated a high degree of crystallinity. This suggests that the barium atoms (which dominate the x-ray scattering) are not much disturbed by these small proton doses. All of the evidence seems to be consistent with the easy formation of interstitial oxygen un-

der proton irradiation.

B. Measurements on Tetragonal Phase $(T < T_C)$

For the measurements on the ferroelectrically polarized phase of $BaTiO_3$, the target crystals were mounted as shown in Fig. 23 and were first heated above the Curie point (to about 150 °C). The star pattern for channeling along the [100] direction was then observed on a ZnS screen. The two strong channeling lines due to the perpendicularly intersecting {100} planes were clearly visible. A dc electric field of about 15 kV/cm was then applied across the crystal in a direction corresponding to one of these {100} planes (shown as vertical in Fig. 23). This had no observable effect on the star pattern. The heater power was then turned off and the crystal was observed with a polarizing microscope (Fig. 6). As the target temperature dropped through the Curie point, the phase transition was easily observable optically. Usually a single ferroelectric a domain resulted. Occasionally a target crystal would refuse to polarize into a single domain, in which case it was discarded. The measurements on the polarized crystals were performed at room temperature. On viewing the star pattern again on the ZnS screen, it was then found to contain only one strong line, corresponding to the {100} plane parallel to the direction of polarization. The pattern showed no evidence of either the [100] axis or the {100} plane perpendicular to the polarization. (Throughout this section, the "{100} planes" will be understood to be the pseudo-{100} planes that correspond to the true {100} planes of the cubic phase.)

Because of the extreme sensitivity to radiation damage in the polarized phase, only measurements with the XY detector (which required small beam currents) were feasible.

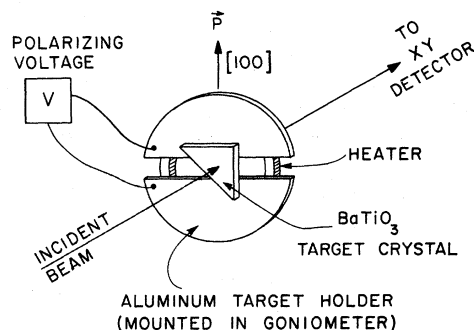Figure 24 shows the result of goniometer scans (similar to the one shown second from the top in

FIG. 23. The target holder, heater, polarizing electrodes, etc., used to obtain single-domain crystals of polarized $BaTiO_3$.
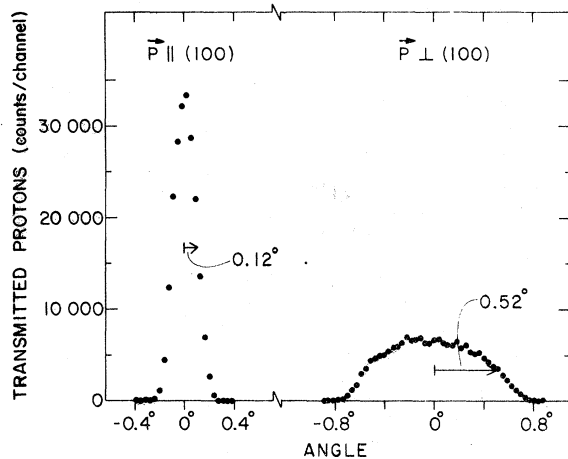
FIG. 24. Angular scan over the proton beam channeled along the (100) planes of BaTiO₃ with its polarization vector $\vec{P}$ polarized either parallel (left) or perpendicular (right) to the (100) planes. As in the next to the top plot in Fig. 11, these data were obtained with the XY detector fixed while the goniometer was scanned in angle relative to the beam direction. The two sets of data were obtained with equal incident proton fluences.

Fig. 11) over {100} planes for the cases in which the polarization is (a) parallel to and (b) perpendicular to the channeling plane. These measurements confirm the effect seen on the ZnS screen.

In an attempt to eliminate the possibility that these observations are due to some spurious effect, the measurements were repeated with several crystals from different batches. Whenever single-domain crystals were used, the observed effect was present. When multidomain crystals were used, a variety of effects were to be seen— the most common being the splitting of the planar patterns into several lines spaced a few tenths of a degree apart. This latter effect was attributed to the crystal twinning at the domain boundaries. The most difficult possibility to eliminate was that the crystals may somehow warp or strain in making the transition from the cubic to the tetragonal phase. Any such warping, however, was not observable directly by examining the crystals. This, together with the fact that the effect was observed with a great variety of crystals with differing thicknesses, production conditions, and mounting arrangements, leads us to believe that warping of the target is an improbable cause of the effect.

In discussing this phenomenon it is useful to refer to Fig. 3, in which the positions of the atoms in a unit cell of tetragonally polarized BaTiO₃ are projected onto one of the {100} planes containing the polarization vector $\vec{P}$. The lattice parameters and atomic displacements are taken from Frazer et al.[6] and Jona and Shirane.[35] It is generally

accepted[36] that the large spontaneous ferroelectric polarization in the tetragonal phase of BaTiO₃ is mostly a consequence of the strong interaction between the titanium and the O_I ions. The axial dipolar fields of these ions acting on each other cause the establishment of dipole chains in the direction of the c axis. In Slater's elementary theory[37] of BaTiO₃, most of the polarization in the tetragonal phase is attributed to the O_I ions (which contribute 59% of the total polarization by virtue of their strong electronic polarization) and to the Ti ions (which contribute 31% of the total by virtue of their ionic polarization). Slater makes the assumption that only the Ti ions are free to be displaced.

In the polarized phase the thermal vibration amplitudes in BaTiO₃ become anisotropic,[11,35] but at room temperature the amplitudes in all directions are smaller than those above the Curie point.

One can readily understand that the channeling properties of the pseudo-{100} planes parallel to the polarization vector would remain strong because there is no displacement of atoms into the channel and the electric field due to the polarization has its major component parallel to the channeling direction. The fields inside the channels are also not extraordinarily large.

For those {100} planes that are at right angles to the polarization vector, the atoms in the channel walls are displaced slightly. Figure 25 shows the continuum planar potential that one then calculates by summing potentials in a way similar to that for the potentials given in Fig. 13. The shape of the potential for the polarized phase (right) is certainly different from that of the unpolarized phase (left), but the difference is not enough to explain the absence of channeling.

Nelson[38] has made a theoretical study of the effect of internal electric fields on the axial channeling of protons along the [100] directions in the rocksalt and cesium chloride structures. In the former, the sign of the ionic charge alternates along a given [100] row. The resultant "quadrupole-lens" effect is calculated to be small for MeV protons. In the cesium chloride structure, however, the individual [100] rows contain only one atomic species. Nelson shows that an annular potential well surrounds each negative-ion row. He concludes that also in this structure the trajectories of MeV protons would only be slightly affected.

It would seem then that the experimentally observed fact that channeling in the {100} planes of BaTiO₃ diminishes when $\vec{P}$ is perpendicular to the planes can best be understood in terms of the extremely high electric fields at right angles to the channel. The magnitudes of these fields between atoms have neither been measured nor calculated for BaTiO₃ as far as we have been able to ascertain. That the fields inside BaTiO₃ may be large
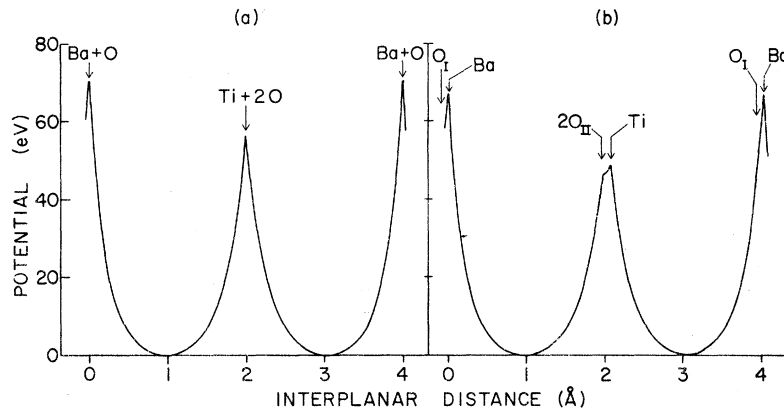
FIG. 25. Interplanar potentials calculated (by use of Lindhard's potential, Ref. 12) for the {100} planes of $BaTiO_3$ (a) in its cubic phase and (b) in the tetragonal phase with neutral unpolarized atoms. Further details are given in the text.

is apparent when one considers that the Lorentz field $\frac{4}{3}\pi\vec{P}$ calculated for a spherical cavity in a continuous homogeneous dielectric medium having a polarization equal to that of tetragonal $BaTiO_3$ (26 $\mu C/cm^2$ at room temperature) is 10^8 V/cm. Of course, $BaTiO_3$ is not continuous and homogeneous, so it may be supposed that the internal crystalline fields assume values higher or lower than 10^8 V/cm depending on the exact position in the lattice. We have made some rough calculations in an attempt to evaluate these local fields. In one simple approach, we have calculated the fields that are produced in the channel by point electric dipoles and point charges located at the lattice sites indicated in Fig. 3. The values for the strengths of the dipoles and charges were taken to be the electronic polarizations and the ionic charges given by Fontaine[39] for $BaTiO_3$. These admittedly crude calculations indicate that the electric field between the ions in the Ti-O_I dipole chains attains values as high as a few times 10^9 V/cm. Fields of this magnitude are sufficiently large that if they were to influence particle trajectories over distances of the order of 1 Å, they could alter the transverse energy of the particle by an amount comparable with the critical transverse energy for channeling. The cross section presented to the beam by these high-field regions is large ($\sim 10^{-17}$ cm^2). It thus seems likely that the initially channeled beam could be rapidly dechanneled by virtue of frequent "collisions" with these high fields, which would cause the transverse energy of the particles to grow faster than it does in the nonpolarized cubic phase.

IV. CONCLUSIONS

In its cubic phase $BaTiO_3$ provides a good test for theories describing channeling in polyatomic crystals. The calculated values of $\psi_{1/2}$ and χ_{min} (Tables II and III), while qualitatively reproducing many of the features of the measured values, do not fit the data as well as do the corresponding ex-

pressions calculated by Barrett[1] for monatomic lattices. This may, in part, be due to oversimplifications implicit in our rather arbitrary interpretations of Barrett's formulas. That simplified interpretations of this sort may be in error has been demonstrated, for example, by the experiments of Altman et al.[40] These authors showed that for planar channeling the simple interpretation that χ_{min} is the initially dechanneled fraction is in error by about a factor of 3. The explanation advanced for the discrepancy is based on the greatly enhanced encounter probability for a large part of those ions that are initially not channeled. This result suggests that interpretations based on simplified geometrical models should be treated with caution.

In order to make comparisons with a more refined model for channeling in polyatomic lattices, it is desirable to obtain more data on a variety of target crystals. Measurements for this purpose are currently in progress at Argonne.

The measurements reported here for temperatures below the Curie point represent the first attempts to examine the interaction between channeling and ferroelectricity. Very strong effects are observed. It would be of interest to extend these measurements to other crystal orientations, thicknesses, etc., and to include backscattering. Formidable experimental problems are raised by the high susceptibility to radiation damage. Possibly these problems may be less severe in some other ferroelectrics that would nevertheless have some of the desirable characteristics of $BaTiO_3$ (e. g., an easily accessible Curie temperature, a simple structure, a high spontaneous polarization, and ferroelectric properties that are fairly well understood theoretically).

ACKNOWLEDGMENT

*Work performed under the auspices of the U. S. Atomic Energy Commission.

†On leave from Macalester College, St. Paul, Minn.

[1] J. H. Barrett, Phys. Rev. B **3**, 1527 (1971).

[2] See, for example, S. T. Picraux, J. A. Davies, L. Eriksson, N. G. E. Johansson, and J. W. Mayer, Phys. Rev. **180**, 873 (1969); F. Abel, G. Amsel, M. Bruneaux, and E. d'Artemare, J. Phys. Chem. Solids **30**, 687 (1969); L. Eriksson and J. A. Davies, Arkiv Fysik **39**, 439 (1969); R. Hellborg, in *Atomic Collision Phenomena in Solids* (North-Holland, Amsterdam, 1970), p. 434.

[3] R. G. Rhodes, Acta Cryst. **4**, 105 (1951).

[4] B. G. Akhmetova, Yu. M. Plets, and A. F. Tulinov, Zh. Eksperim. i Teor. Fiz. **56**, 813 (1969) [Sov. Phys. JETP **29**, 442 (1969)].

[5] H. D. Megaw, *Ferroelectricity in Crystals* (Methuen, London, 1957).

[6] B. C. Frazer, H. Danner, and R. Pepinsky, Phys. Rev. **100**, 745 (1955).

[7] *Proceedings of the International Conference on Atomic Collision Phenomena in Solids, Gausdal, Norway*, 20–24 *September*, 1971, Radiation Effects **12**, 1 (1972).

[8] D. S. Gemmell and J. N. Worthington, Nucl. Instr. Methods **91**, 15 (1971).

[9] J. P. Remeika, J. Am. Chem. Soc. **76**, 940 (1954).

[10] See, for example, C. Erginsoy, Phys. Rev. Letters **15**, 360 (1965). In evaluating the Molière potentials, we have used Eq. (3a) from Barrett (Ref. 1) to calculate Thomas-Fermi radii.

[11] T. Pedersen, J. Phys. Soc. Japan **29**, 1314 (1970).

[12] J. Lindhard, Kgl. Danske Videnskab. Selskab, Mat.-Fys. Medd. **34**, No. 14 (1965).

[13] J. U. Anderson, Kgl. Danske Videnskab. Selskab, Mat.-Fys. Medd. **36**, No. 7 (1967).

[14] J. C. Poizat and J. Remillieux, Phys. Rev. Letters **27**, 6 (1971).

[15] G. A. Bissinger, J. M. Joyce, E. J. Ludwig, W. S. McEver, and S. M. Shafroth, Phys. Rev. A **1**, 841 (1970).

[16] S. Roth, R. Sizmann, R. Coutelle, and F. Bell, Phys. Letters **32A**, 119 (1970).

[17] See, for example, S. Datz, C. Erginsoy, G. Leibfried, and H. O. Lutz, Ann. Rev. Nucl. Sci. **17**, 129 (1967).

[18] B. R. Appleton, C. Erginsoy, and W. M. Gibson, Phys. Rev. **161**, 330 (1967).

[19] See, for example, B. R. Appleton, J. H. Barrett, T. S. Noggle, and C. D. Moak, in Ref. 7.

[20] J. A. Davies, J. Denhartog, and J. L. Whitton, Phys. Rev. **165**, 345 (1968).

[21] G. Foti, F. Grasso, R. Quattrocchi, and E. Rimini, Phys. Rev. B **3**, 2169 (1971).

[22] E. Bonderup, H. Esbensen, J. U. Andersen, and H. E. Schiøtt, in Ref. 7.

[23] K. Morita and N. Itoh, J. Phys. Soc. Japan **30**, 1430 (1971).

[24] C. F. Williamson, J.-P. Boujot, and J. Picard, Saclay Report R3042 (unpublished).

[25] L. C. Feldman, B. R. Appleton, and W. L. Brown, in Proceedings of the International Conference on Solid State Physics Research with Accelerators, Brookhaven National Laboratory Report BNL 50083, p. 58 (1967) (unpublished).

[26] R. D. Edge and R. L. Dixon, in *Atomic Collision Phenomena in Solids* (North-Holland, Amsterdam, 1970), p. 435.

[27] See, for example, R. W. Harris, G. C. Philips, and C. Miller Jones, Nucl. Phys. **38**, 259 (1962).

[28] K. Morita, K. Tachibana, and N. Itoh, Phys. Letters **33A**, 257 (1970).

[29] D. D. Glower and D. L. Hester, J. Appl. Phys. **36**, 2175 (1965).

[30] S. P. Solov'ov, I. I. Kuz'min, and V. A. Kharchenko, Bull. Acad. Sci. (USSR) **31**, 1799 (1967).

[31] I. I. Kuz'min, S. P. Solov'ov, and V. V. Zakurkin, Bull. Acad. Sci. (USSR) **33**, 326 (1969).

[32] M. C. Wittels and F. A. Sherrill, J. Appl. Phys. **28**, 606 (1957).

[33] J. J. Keating and G. Murphy, Phys. Rev. **184**, 476 (1969).

[34] See, for example, D. Van Vliet, Radiation Effects **10**, 137 (1971).

[35] F. Jona and G. Shirane, *Ferroelectric Crystals* (Pergamon, London, 1962).

[36] See, for example, the discussions by E. Fatuzzo and W. J. Mertz, *Ferroelectricity* (Interscience, Amsterdam, 1967), and references therein.

[37] J. C. Slater, Phys. Rev. **78**, 748 (1950).

[38] R. S. Nelson, Phil. Mag. **14**, 637 (1966).

[39] G. Fontaine, J. Phys. Chem. Solids **28**, 2199 (1967).

[40] M. R. Altman, L. C. Feldman, and W. M. Gibson, Phys. Rev. Letters **24**, 464 (1970).